The C7orf43/TRAPPC14 component links the TRAPPII complex to Rabin8 for preciliary vesicle tethering at the mother centriole during ciliogenesis

Received for publication, March 26, 2019, and in revised form, August 25, 2019 Published, Papers in Press, August 29, 2019, DOI 10.1074/jbc.RA119.008615

Adrian Cuenca[‡], Christine Insinna[‡], Huijie Zhao[‡], Peter John[‡], Matthew A. Weiss[‡], Quanlong Lu[‡], Vijay Walia[‡], Suzanne Specht[‡], Selvambigai Manivannan[§1], Jimmy Stauffer[‡], Andrew A. Peden[§1], and Christopher J. Westlake[‡2]

From the [‡]Center for Cancer Research, NCI-Frederick, National Institutes of Health, Laboratory of Cellular and Developmental Signaling, Frederick, Maryland 21702 and the [§]Department of Biomedical Sciences, University of Sheffield, Sheffield S10 2TN, United Kingdom

Edited by Peter Cresswell

The primary cilium is a cellular sensor that detects light, chemicals, and movement and is important for morphogen and growth factor signaling. The small GTPase Rab11–Rab8 cascade is required for ciliogenesis. Rab11 traffics the guanine nucleotide exchange factor (GEF) Rabin8 to the centrosome to activate Rab8, needed for ciliary growth. Rabin8 also requires the transport particle protein complex (TRAPPC) proteins for centrosome recruitment during ciliogenesis. Here, using an MS-based approach for identifying Rabin8-interacting proteins, we identified C7orf43 (also known as microtubule-associated protein 11 (MAP11)) as being required for ciliation both in human cells and zebrafish embryos. We find that C7orf43 directly binds to Rabin8 and that C7orf43 knockdown diminishes Rabin8 preciliary centrosome accumulation. Interestingly, we found that C7orf43 co-sediments with TRAPPII complex subunits and directly interacts with TRAPPC proteins. Our findings establish that C7orf43 is a TRAPPII-specific complex component, referred to here as TRAPPC14. Additionally, we show that TRAPPC14 is dispensable for TRAPPII complex integrity but mediates Rabin8 association with the TRAPPII complex. Finally, we demonstrate that TRAPPC14 interacts with the distal appendage proteins Fas-binding factor 1 (FBF1) and centrosomal protein 83 (CEP83), which we show here are required for GFP-Rabin8 centrosomal accumulation, supporting a role for the TRAPPII complex in tethering preciliary vesicles to the mother centriole during ciliogenesis. In summary, our findings have revealed an uncharacterized TRAPPII-specific component, C7orf43/TRAPPC14, that regulates preciliary trafficking of Rabin8 and ciliogenesis and support previous findings that the TRAPPII complex functions as a membrane tether.

The primary cilium serves as a cellular sensory antennae detecting light, chemicals, and movement and is important for morphogen and growth factor signaling (1). Genetic disorders, referred to as ciliopathies, and certain forms of cancer are associated with defects in ciliogenesis and functionality of the cilium (1, 2). Cilia formation can occur, in part, inside the cell and requires dynamic vesicular membrane trafficking processes, including transport, docking, and fusion at the distal end of the mother centriole (MC),[3] prior to axonemal growth (3, 4). Small membrane vesicles, or distal appendage vesicles, dock to the MC distal appendage proteins (DAPs) and subsequently fuse into a larger ciliary vesicle (5, 6). This membrane ensheaths the developing axoneme and facilitates fusion with the plasma membrane, a process that involves membrane tubulation (6). The small GTPase membrane trafficking regulator Rab family members Rab8, Rab10, Rab11, and Rab34 have been reported to function in ciliogenesis, along with the membrane fusion SNARE SNAP29 and membrane organizer/reshaping EHD and PACSIN proteins (5–12). Large trafficking regulator complexes such as the exocyst and TRAPPII complex are also required for ciliogenesis (9, 13–15).

A Rab11-Rab8 cascade functions in ciliogenesis, wherein Rab11 traffics the guanine nucleotide exchange factor (GEF) Rabin8 to the MC to activate Rab8 to the GTP state for its required function in axonemal growth (5, 7, 9). In addition to its role in ciliogenesis, this Rab cascade has also been described to function in apical membrane formation (16), and has been implicated in immune synapse transport (17). This Rab cascade is conserved in yeast and involves the Rab11 orthologues Ypt31p/Ypt32p recruiting the GEF Sec2 to activate Sec4 needed for neck bud formation (18).

Notably, Rab11-dependent Rabin8 preciliary trafficking to the centrosome is the earliest ciliogenesis process that has been described, observable within minutes of serum starvation (9),

This research was supported by the Intramural Research Program of NCI, National Institutes of Health. The authors declare that they have no conflicts of interest with the contents of this article. The content is solely the responsibility of the authors and does not necessarily represent the official views of the National Institutes of Health.
This article contains Table S1 and Figs. S1–S7.
[1] Supported by Biotechnology and Biological Sciences Research Council UK Grant BB/L002841/1.
[2] To whom correspondence should be addressed. E-mail: chris.westlake@nih.gov.

[3] The abbreviations used are: MC, mother centriole; GEF, guanine nucleotide exchange factor; TRAPPC, transport particle protein complex; DAP, distal appendages; NeoHDF, neonatal human dermal fibroblasts; RPE-1, retinal pigment epithelial; LAP, localization affinity purification; TAP, tandem affinity purification; mIMCD3, mouse inner medullary collecting duct; PSM, peptide-spectrum match; MW, molecular weight; [Ac]tub, acetylated tubulin; dpf, days postfertilization; HA, hemagglutinin; MO, morpholino; MCPH, microcephaly; HRP, horseradish peroxidase; NP-40, Nonidet P-40; WCL, whole-cell lysate.

which promotes cilia assembly in cultured RPE-1 cells (11). This preciliary trafficking is regulated by lysophosphatidic acid signaling through Akt to control a Rab11-effector switch from Rab11-WDR44 to the ciliogenic Rab11-FIP3-Rabin8 trimeric complex (19). Interestingly, Rabin8 trafficking is reduced after cilia formation (9, 15), presumably limiting Rab8 activation and could be important for cilia length control. This regulation involves the phosphorylation of Rabin8 on Ser^{272} by the NDR2 kinase, shifting its affinity from phosphatidylserine on Rab11-positive vesicles to Sec15 for its retention on the MC (15). However, it is not clear how these preciliary vesicles are recruited to the MC, although Rabin8 has been reported to interact with the DAP protein Cep164 (20). Our previous studies demonstrated that ablation of TRAPPC proteins reduces Rabin8 accumulation at the centrosome, suggestive of a role for the TRAPPII complex in regulating transport and/or tethering of preciliary vesicles to the MC during ciliogenesis (9). TRAPPIII-specific components have also been shown to be important for GFP-Rabin8 localization to the centrosome and ciliogenesis (21). Mutations in both TRAPPII and TRAPPIII complex proteins have been identified in neurodevelopmental disorders involving microcephaly and intellectual disabilities (22), diseases linked to ciliopathy (23–26).

There have been as many as four TRAPP complexes described as TRAPPI, -II, -III, and -IV (27–30). The "core" TRAPPC proteins, thought to include the TRAPPI complex, include TRAPPC1–6. The TRAPPII complex comprises the core proteins and Trs120/TRAPPC9, Trs130/TRAPPC10, and in yeast, Trs65. In mammals, C5orf44/TRAPPC13 has been proposed to be the homologue of Trs65 (31), but it was recently shown to associate and function with the TRAPPIII complex (32, 33). The yeast TRAPPIII complex consists of the core plus Trs85/TRAPPC8 (28), whereas TRAPPC11 and TRAPPC12 are included in the mammalian TRAPPIII complex, along with TRAPPC13 (34). The TRAPPII complex is thought to function in late Golgi trafficking, and TRAPPIII has been implicated in both endoplasmic reticulum-to-Golgi transport and autophagy (22). In yeast, the TRAPPII complex has been observed to have GEF activity for Ypt1 and Ypt31p/Ypt32 (35–37), the respective human homologues of Rab1 and Rab11. Likewise, in *Drosophila*, TRAPPII has been shown to have GEF activity toward Rab1 and Rab11 (38). In contrast, the mammalian TRAPPII complex was reported to have GEF activity toward Rab1, but not Rab11 (39). The TRAPP complexes have also been described to function as molecular tether factors in membrane fusion (29, 40–42); however, this function is less well-understood compared with its GEF activity.

In the present study, we have further investigated Rabin8 preciliary trafficking regulation during ciliogenesis by seeking to identify and characterize novel Rabin8-interacting proteins. By comparing MS results of immunoprecipitated Rabin8 from RPE-1 cells with our previous analysis in 293Trex and mouse inner medullary collecting duct (mIMCD3) cells (9), we identified C7orf43 across all three cell lines and showed that it can directly bind to Rabin8. Interestingly, C7orf43 interacts with the N-terminal fragment of Rabin8, similar to the TRAPPII complex (9). We demonstrate that C7orf43 is required for ciliogenesis in human cells and zebrafish embryos. Moreover, we show that C7orf43 colocalizes with Rabin8 on preciliary vesicles and is needed for the accumulation of these membranes at the centrosome, consistent with the ciliogenesis function observed for TRAPPII complex subunits. Biochemical investigation of C7orf43 by MS, immunoprecipitation analysis, size-exclusion chromatography, and yeast two-hybrid analysis indicated that this protein is a TRAPPII complex component, TRAPPC14, possibly the yeast Trs65 orthologue. We show that TRAPPC14 interaction with this complex depends on TRAPPC9 and -C10, but TRAPPC14 is dispensable for the assembly/stability of the TRAPPII complex. Notably, TRAPPC14 is essential for Rabin8 association with the TRAPPII complex. Furthermore, we show that TRAPPC14 binds DAP proteins needed for GFP-Rabin8 accumulation at the centrosome, evidence that TRAPPC14 and the TRAPPII complex functions to tether preciliary vesicles to the MC during ciliogenesis.

Results

Identification of C7orf43 interaction with Rabin8

Given the observation that GFP-Rabin8 trafficking to the centrosome precedes Rab8-dependent primary cilia growth in human retinal pigment epithelial (RPE-1) cells (7, 9), which use the intracellular ciliogenesis pathway (43), we sought to understand better how this transport process is controlled. Previously, the localization affinity purification (LAP) tag containing GFP and S peptide (S-tag) fused to Rabin8 was used to perform tandem affinity purification (TAP) and MS in human 293Trex Flp-In and mIMCD3 Flp-In cells (9). Here, we described a similar immunoprecipitation and MS approach using LAP-Rabin8 expressed in the RPE-1 Flp-In cell line. We identified the same components of the TRAPPII complex in RPE-1 Flp-In cells as observed in 293Trex Flp-In and mIMCD3 Flp-In cells (Fig. 1*A*). Interestingly, C7orf43 was detected in all three cell lines with 6, 14, and 21 unique peptides detected in RPE-1, mIMCD3, and 293Trex Flp-In cells, respectively, covering 9.7, 7.2, and 33% of the protein's peptide sequence (%*C*) (Fig. 1*A*). Together, these results show that Rabin8 biochemical interactions are largely conserved across the cell lines, and, using this approach, we identified a potential novel Rabin8-interacting protein.

Based on these findings, we further investigated Rabin8 interaction with C7orf43 by performing co-expression co-immunoprecipitation studies. Consistent with the MS results, HA-tagged C7orf43 bound to GFP-Rabin8 (Fig. 1*B*), but not to GFP alone, indicating that this interaction is specific. To test whether this interaction is direct, we expressed His-C7orf43 and GST-Rabin8 in *Escherichia coli*. His-tagged C7orf43 from *E. coli* lysate displayed binding to immobilized GST-Rabin8 but did not bind to GST alone, indicating that these proteins bind directly (Fig. 1*C*). Consistent with these results, transiently expressed and immunoprecipitated C7orf43-LAP could pull down GST-Rabin8, but not GST alone (Fig. S1*A*). Interestingly, C7orf43-LAP binding to GST-Rabin8 was similar to binding to constitutively active GFP-Rab11a Q70L and stronger than to the GDP form of GFP-Rab11aS25N (Fig. S1*B*). Together, these results indicate that Rabin8 binds directly to C7orf43.

A

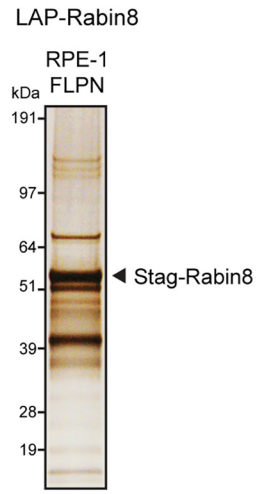

MW	Protein	RPE-1 Flp-In LAP-Rabin8 UP	RPE-1 Flp-In LAP-Rabin8 %C	mIMCD3 Flp-In LAP-Rabin8 UP	mIMCD3 Flp-In LAP-Rabin8 %C	293Trex Flp-In LAP-Rabin8 UP	293Trex Flp-In LAP-Rabin8 %C	293Trex Flp-In LAP-Rabin8$_{1-142}$ UP	293Trex Flp-In LAP-Rabin8$_{1-142}$ %C
51	Rabin8	39	65	31	43	47	68	7	na
63	C7orf43	6	9.7	14	7.2	21	33	16	29
17	TRAPPC1	5	26	16	84	9	61	8	50
16	TRAPPC2	2	16	15	67	15	76	4	29
16	TRAPPC2L	5	25	17	78	17	73	5	27
20	TRAPPC3	8	37	17	54	16	46	9	38
24	TRAPPC4	8	35	19	79	24	79	10	37
21	TRAPPC5	5	20	16	79	12	62	6	23
18	TRAPPC6A/B	-/4	-/16	-/16	-/59	1/15	5.7/65	1/10	4/47
128	TRAPPC9	17	12	67	58	75	51	39	24
142	TRAPPC10	12	6.6	43	35	172	49	35	28
161	TRAPPC8	-	-	-	-	-	-	-	-
129	TRAPPC11	-	-	-	-	-	-	-	-
79	TRAPPC12	-	-	-	-	-	-	-	-

B

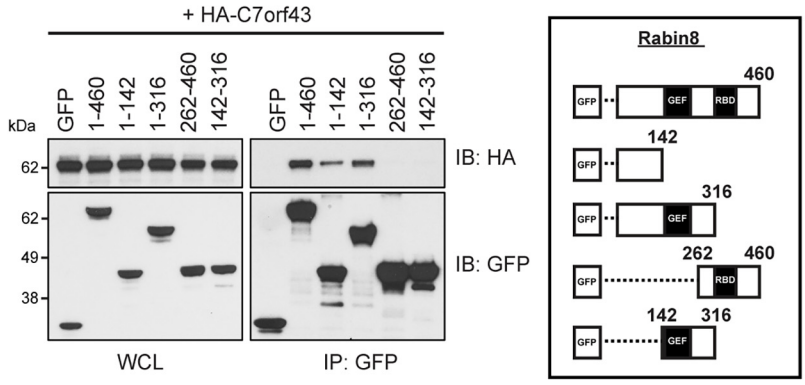

C

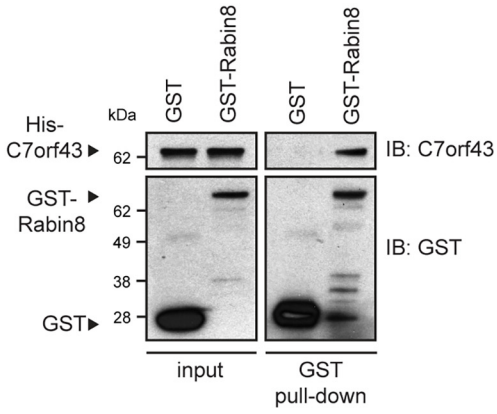

D

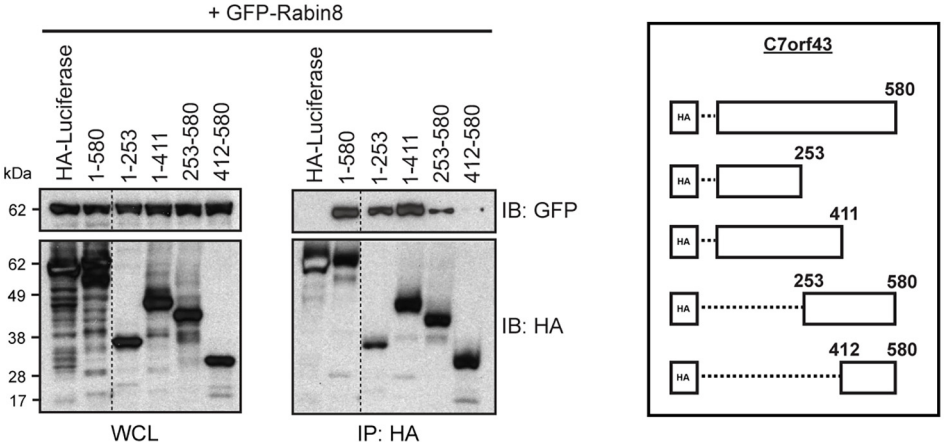

Figure 1. C7orf43 binds to the N-terminal region of Rabin8. *A*, *left*, silver stain of SDS-polyacrylamide gel (4–12% gradient) of LAP-tagged Rabin8 purified by TAP (anti-GFP antibodies, followed by S-tag beads) from RPE-1 Flp-In stably expressing cells. 14 equally spaced gel slices were cut and analyzed by LC-MS/MS from a single experiment. *Right*, full-length Rabin8– and Rabin8$_{1-142}$–associated proteins and TRAPPCII components and C7orf43 had high-percentage peptide coverage in gel slices analyzed by LC-MS/MS corresponding to their predicted molecular weight from RPE-1 and 293Trex cells. Shown is MS analysis of full-length Rabin8 from mIMCD3 and HEK293Trex cells and Rabin8$_{1-142}$ from HEK293Trex from Ref. 9. *UP*, unique peptides; %*C*, percentage of amino acid coverage from peptides identified. *B*, domain mapping of Rabin8 for C7orf43 binding. *Left*, GFP antibody immunoprecipitation (*IP*) of GFP-Rabin8 WT and truncated fragments with HA-C7orf43 co-expressed in HEK293 cells for 48 h. Blots were probed with HA and GFP antibodies. Representative results from four independent experiments are shown. *Right*, *schematic representation* of GFP-Rabin8 full-length and deletion constructs used in immunoprecipitation. *C*, *in vitro* binding assay pull-down of recombinant His-tagged C7orf43 by GST and GST-Rabin8. Representative results from two independent experiments are shown. *D*, domain mapping of C7orf43 binding to Rabin8. *Left*, HA-beads were used to immunoprecipitate GFP-Rabin8 using HA-tagged C7orf43 full-length and deletion fragments. Representative results from two independent experiments are shown. *Right*, *schematic representation* of HA-C7orf43 full-length and deletion constructs used.

We next investigated protein sequence requirements for interaction between Rabin8 and C7orf43. HA-C7orf43 specifically immunoprecipitated with the N-terminal 142 amino acids of Rabin8 but not with C-terminal fragments (Fig. 1*B*), which contain the GEF- and Rab11-interacting domains (7, 9). Examination of TAP-MS results using a truncated GFP-Rabin8$_{1-142}$ protein from 293Trex Flp-In cells also revealed the presence of C7orf43 (Fig. 1*A*). The Rabin8 N-terminal region was previously shown to associate with the TRAPPII complex (9). We next performed reciprocal immunoprecipitation analysis with HA-C7orf43 fragments and demonstrated that GFP-Rabin8 preferentially binds more strongly to the N-terminal fragments of C7orf43 (C7orf43$_{1-253}$ and C7orf43$_{1-411}$) than the C-terminal fragment (C7orf43$_{253-580}$), whereas a fragment containing the final 168 amino acids displayed no binding to Rabin8 (C7orf43$_{412-580}$) (Fig. 1*D*). These results suggest that elements in the first 411 amino acids of C7orf43 are involved in interaction with Rabin8. DELTA-BLAST analysis for C7orf43 identifies a conserved domain of unknown function, DUF4707, spanning residues 139–579 (Figs. S2 and S3). Together, our immunoprecipitation results indicate that C7orf43 and Rabin8 interactions are mediated by elements in the N-terminal region of each protein.

C7orf43 is required for ciliogenesis in human cells and zebrafish embryos

Because Rabin8 is required for ciliogenesis (11), we investigated the effects of C7orf43 ablation on ciliation. Two C7orf43 siRNAs were identified, which knocked down the protein by >80% (Fig. 2*A*), with the strongest reduction in C7orf43 protein observed following treatment with both siRNA oligonucleotides. Analysis of ciliation levels in neonatal human dermal fibroblasts (NeoHDF) demonstrated a requirement for C7orf43 in ciliogenesis and correlated with the knockdown levels of the protein (Fig. 2, *A* and *B*). In C7orf43 siRNA#1+#2–treated cells, ciliation was observed in 32 ± 4.52% (mean ± S.E.) of cells, whereas 62 ± 4% of siControl-treated cells had cilia. Ciliogenesis was also reduced in RPE-1 cells following C7orf43 siRNA treatment (47 ± 3.6%) compared with siControl (65 ± 3.23%) (Fig. 2*C*). Together, these results indicate that C7orf43 is important for ciliogenesis in human cells.

To further investigate C7orf43 ciliogenesis requirements, we performed morpholino (MO) knockdowns of *c7orf43* in zebrafish embryos. Suppression of C7orf43 was confirmed by Western blotting (Fig. 2*D*). Two-day-old embryos injected with *c7orf43* MO demonstrated curved bodies (41% in MO-treated compared with 10% in control) and small eyes (38% in MO-treated compared with 8% in control) (Fig. 2*E*), defects consistent with genes known to affect ciliogenesis (44). As observed in mammalian cells, *c7orf43* morphants exhibited reduced ciliation (Fig. 2, *F–H*) in otic vesicles, neuromasts, and olfactory placodes. Human C7orf43 mRNA successfully rescued both morphological (curved bodies, 33% MO + rescue; small eyes, 11% MO + rescue) and ciliogenesis defects (Fig. 2, *F–H*), validating that the MO effects observed are specific to *c7orf43*. Together, these results indicate that C7orf43 is required for cilia formation in human cells and zebrafish embryos.

C7orf43 colocalizes with Rabin8 on preciliary vesicles and is required for Rabin8 preciliary vesicle accumulation at the centrosome

Previously, we showed that Rabin8 accumulates at the centrosome in the majority of cells within 1 h of serum starvation (9). To determine whether C7orf43 is associated with Rabin8 preciliary trafficking, we co-expressed N-terminal and C-terminal LAP-tagged C7orf43 with tRFP-Rabin8 in RPE-1 cells to examine their subcellular distribution. In serum-fed cells, both proteins appeared diffuse throughout the cytoplasm in most cells (Fig. 3*A* and Fig. S4*A*), but, following 1-h serum starvation, these proteins colocalized more on vesicles (Fig. 3 (*A* and *B*) and Fig. S4*B*). We also examined C7orf43-LAP localization on its own and observed this protein in the cytoplasm (Fig. 3*B* and Fig. S4*A*), with some cells showing vesicular localization that partially overlapped with the Golgi marker GM130 (Fig. S4*A*). C7orf43 and Rabin8 did not colocalize on pericentriolar vesicles with myosin-Va (Fig. S4*B*), a vesicular trafficking regulator of early ciliary assembly (45). This result is consistent with myosin-Va and Rabin8 involvement with discrete ciliogenesis functions. Furthermore, as has been reported previously for Rabin8 (9, 15), pericentrosomal vesicular Rabin8-C7orf43 was not observed in ciliated cells (Fig. 3*B* and Fig. S4*C*). Interestingly, Rabin8 and C7orf43 colocalized in the cilium in rare instances (Fig. S4*C*), suggestive of their accumulation in newly formed cilia. Similarly, Rab8 accumulates in growing cilia and is later lost from cilia after organelle assembly (9). Together, these results suggest that C7orf43 ciliogenic requirements may be associated with Rabin8 preciliary trafficking.

To investigate whether C7orf43 is important for Rabin8 preciliary trafficking, we performed RNAi knockdowns in RPE-1 cells expressing GFP-Rabin8 and monitored preciliary trafficking in live cells following 1–2-h serum starvation (Fig. 3 (*C* and *D*) and Fig. S4*D*). Strikingly, cells depleted of C7orf43 showed reduced GFP-Rabin8 focal accumulation in the centrosomal region compared with siControl treated cells. As was observed with ciliation (Fig. 2*B*), the effects on GFP-Rabin8 centrosomal accumulation correlated with protein knockdown using two independent siRNAs alone and in combination (Fig. 2*A* and Fig. S4*D*). Merged images from GFP-Rabin8–positive vesicles imaged at 0-, 2-, and 4-s time intervals and differentially colored with *red*, *green*, and *blue*, respectively, for these time points showed vesicular transport in the centrosomal region under both treatments, but with more white structures observed in the centrosomal region of the cell in siC7orf43-treated cells, indicating vesicle accumulation and/or nontrafficking membrane compartments (Fig. 3*C*). A small reduction in the number of cells displaying vesicular GFP-Rabin8 throughout the cell was observed in C7orf43 RNAi conditions compared with control (Fig. 3, *C* and *D*). Similar results were observed in experiments performed using RPE-1 cells expressing GFP-Rabin8 and tRFP-Centrin2 (Fig. 3*E*), with tRFP-Centrin2 marking the position of the centrioles. Together, these studies demonstrate that C7orf43 is important for Rabin8 preciliary vesicle trafficking to the centrosome during ciliogenesis.

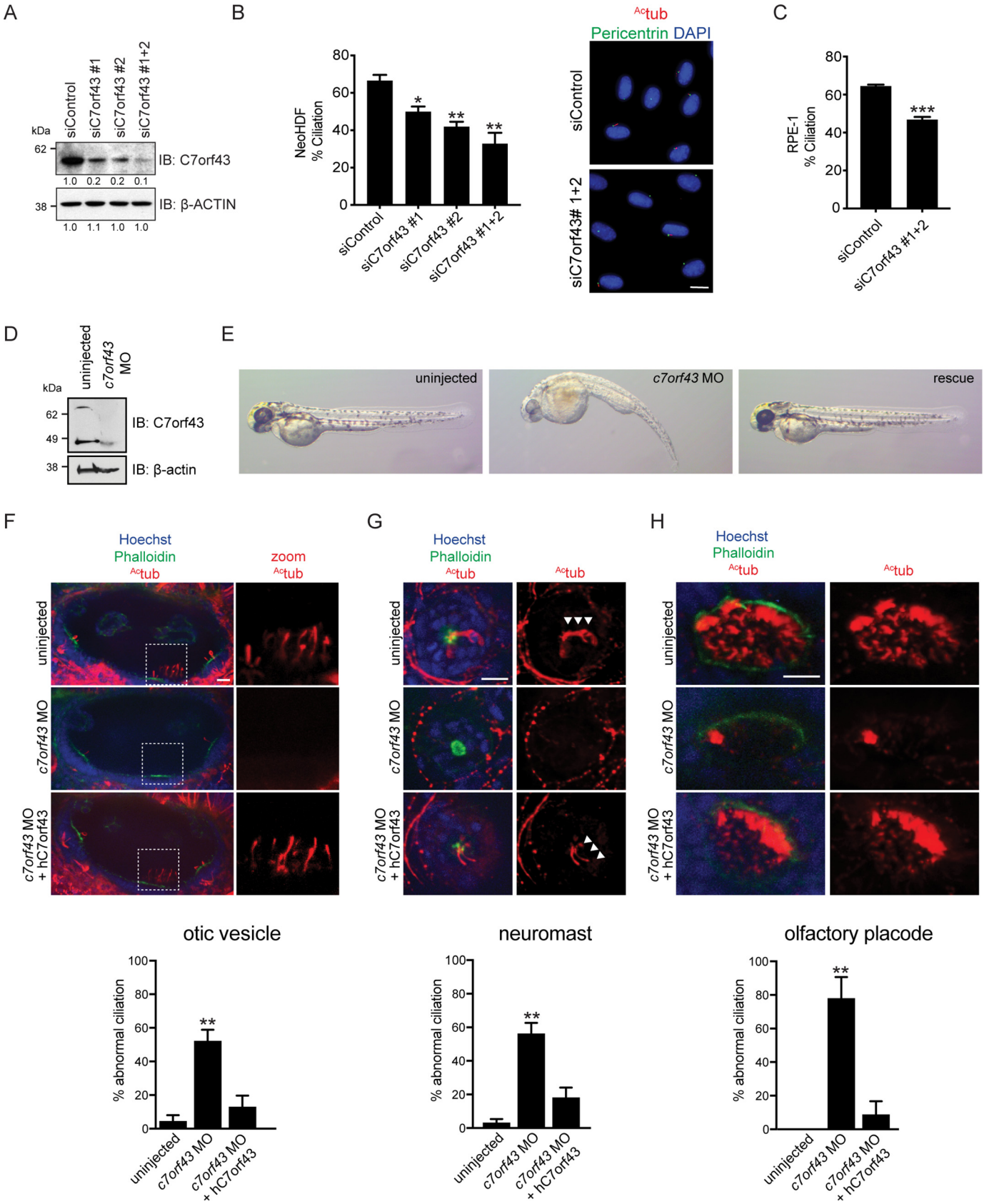
A
siControl
siC7orf43 #1
siC7orf43 #2
siC7orf43 #1+2
kDa
62
IB: C7orf43
1.0 0.2 0.2 0.1
38
IB: β-ACTIN
1.0 1.1 1.0 1.0
B
NeoHDF
% Ciliation
siControl
siC7orf43 #1
siC7orf43 #2
siC7orf43 #1+2
Actub
Pericentrin DAPI
siControl
siC7orf43# 1+2
C
RPE-1
% Ciliation
siControl
siC7orf43 #1+2
D
uninjected
c7orf43 MO
kDa
62
49
IB: C7orf43
38
IB: β-actin
E
uninjected
c7orf43 MO
rescue
F
Hoechst
Phalloidin
Actub
zoom
Actub
uninjected
c7orf43 MO
c7orf43 MO + hC7orf43
G
Hoechst
Phalloidin
Actub
Actub
uninjected
c7orf43 MO
c7orf43 MO + hC7orf43
H
Hoechst
Phalloidin
Actub
Actub
uninjected
c7orf43 MO
c7orf43 MO + hC7orf43
otic vesicle
% abnormal ciliation
uninjected
c7orf43 MO
c7orf43 MO + hC7orf43
neuromast
% abnormal ciliation
uninjected
c7orf43 MO
c7orf43 MO + hC7orf43
olfactory placode
% abnormal ciliation
uninjected
c7orf43 MO
c7orf43 MO + hC7orf43

C7orf43 co-fractionates with high-molecular weight TRAPPII complexes and directly binds to TRAPPC components

To further investigate C7orf43 function, we performed MS analysis on immunoprecipitated C7orf43-LAP. Remarkably, we identified peptides for most of the TRAPPII-complex that were not detected in the LAP control sample (Fig. 4*A*). Likewise, immunoprecipitated native C7orf43 interacted with the TRAPPII proteins tested (Fig. 4*B*). These observations are intriguing, as we previously demonstrated that these TRAPPC proteins bind specifically to the N-terminal fragment of Rabin8 and affect both ciliogenesis and centriolar Rabin8 preciliary vesicle accumulation upon depletion (9). Rabin8 peptides were not detected in C7orf43-LAP MS. Interestingly, TRAPPIII complex subunits were not enriched in C7orf43-LAP MS samples (Fig. 4*A*); nor were they detected in the LAP-Rabin8 analysis (Fig. 1*A*).

To investigate C7orf43 interaction with TRAPPC proteins, we performed immunoprecipitation experiments on TRAPPC10-LAP, a TRAPPII-specific component (Fig. 4*C*). TRAPPC10-LAP bound to endogenous C7orf43, along with the TRAPPII-specific TRAPPC9 protein and the core TRAPPC protein TRAPPC4. These proteins were not detected in control LAP immunoprecipitations (Fig. 4*C*). We also demonstrated that C7orf43 could not be immunoprecipitated with the TRAPPIII-specific complex subunit, TRAPPC11, and, as expected, TRAPPC11 immunoprecipitated TRAPPC4 and did not interact with TRAPPC9 (Fig. 4*C*). Next, we investigated C7orf43 interaction requirements with TRAPPC10. Elements between residues 1 and 411 are required for C7orf43 interaction with TRAPPC10 (Fig. 4*D*), whereas the C-terminal 168 amino acids ($C7orf43_{412-580}$) were dispensable for TRAPPC10 binding. As TRAPPC10 binding was not observed to $C7orf43_{1-253}$ and $C7orf43_{253-580}$ fragments, this suggests that elements in the N-terminal 411 residues must be intact for TRAPP10 binding (Fig. 4*D*). Whereas Rabin8 interaction with C7orf43 is also mediated by elements in the N-terminal 411 residues, unlike TRAPPC10, Rabin8 displayed binding to $C7orf43_{1-253}$ and $C7orf43_{253-580}$ fragments (Fig. 1*D*). Together, these findings show that C7orf43 interacts with TRAPPII complex proteins and suggest that binding requirements in C7orf43 for TRAPPC10 interaction are different from those observed for Rabin8.

To further investigate C7orf43 associations with the TRAPPII complex, both of which localize to the Golgi (Fig. S4*A*) (22), we performed size-exclusion chromatography on HEK293 cell lysates. Strikingly, most of C7orf43 was detected in high-molecular weight (MW) fractions with the TRAPP proteins (Fig. 4*E*). This differs from Rabin8, which was largely associated with smaller-molecular weight fractions, consistent with our previous observations (9). A higher-MW form, correlating with the largest predicted splice form of C7orf43 (~63 kDa) and accounting for ~¼ of the total protein, was spread across the fractions containing TRAPPC proteins and Rabin8. Two slightly smaller but more prominent MW forms co-fractionated at high molecular weights with TRAPPII-specific components, TRAPPC9 and TRAPPC10, and core TRAPP proteins. Thus, these findings in combination with our previous MS analysis suggest that C7orf43 is primarily associated with the TRAPPII complex and, therefore, could be a TRAPPC protein. To further investigate this possibility, we performed yeast two-hybrid studies on C7orf43 with TRAPPC proteins (Fig. 4*F*). Remarkably, C7orf43 fused to the GAL4 DNA-binding domain interacted with TRAPPC2, -C6A, and -C10 fused with the GAL4 activation domain, but not with other TRAPPII components, TRAPPIII-specific TRAPPC11, or the GAL4 activation domain alone. Together, these results suggest that C7orf43 may be an uncharacterized human TRAPPC protein. Interestingly, C7orf43 shows sequence similarity to the yeast TRAPPII protein Trs65 and has a comparable molecular weight (Fig. S5), suggesting that these proteins could be homologs.

C7orf43/TRAPPC14 affects TRAPPII complex size but is dispensable for complex integrity

To further investigate C7orf43 as a TRAPPC protein, we examined its involvement in complex assembly and integrity. Interestingly, both core TRAPP and TRAPPII-specific components shifted to a smaller-molecular weight complex following depletion of C7orf43 compared with control RNAi-treated samples, whereas control actin fractionation was largely unchanged in both conditions (Fig. 5*A*). Considering this together with our other findings, we believe there is enough evidence to conclude that C7orf43 is an uncharacterized mammalian TRAPPII complex protein, which we refer to as TRAPPC14. However, the observation that the TRAPPC components analyzed remained together in high-molecular weight fractions under these conditions suggested that C7orf43/TRAPPC14 is not required for TRAPPII complex assembly or integrity. This conclusion is supported by immunoblotting and MS analysis of immunoprecipitated LAP-TRAPPC10 in cells with and without TRAPPC14, which showed little effect on its interactions with TRAPPC2, -C3, and -C9 proteins and TRAPPC protein peptides numbers detected, respectively

Figure 2. C7orf43 is required for ciliogenesis in human cells and zebrafish embryos. *A*, Western blot analysis of lysates from RPE-1 cells treated with control and C7orf43 siRNAs for 72 h. C7orf43 and β-actin antibodies were used for immunoblotting. Protein levels of C7orf43 compared with siControl were determined by densitometry analysis and are shown *below* blots normalized for differences in actin expression between RNAi treatments. Representative results from three independent experiments are shown. *B* and *C*, quantification of ciliation in NeoHDF (*B*) and RPE-1 (*C*) cells treated with C7orf43 siRNAs as in *A* and serum-starved for the final 24 h. Cells were stained with acetylated tubulin (^{Ac}tub) and pericentrin antibodies and 4′,6-diamidino-2-phenylindole and imaged by epifluorescence microscopy. Representative images (*right*) are shown in *B*. *Scale bar*, 10 μm. Cells were counted for NeoHDF, siControl ($n = 607$) and siC7orf43 ($n = 521$) (*B*). Cells were counted for RPE-1, siControl ($n = 1287$), and siC7orf43 ($n = 1070$) (*C*). Means ± S.E. (*error bars*) are shown from three independent experiments. Two-tailed, unpaired Student's *t* test was used. *, $p < 0.05$; **, $p < 0.01$; ***, $p < 0.001$. *D*, Western blot analysis of lysates from 2-day postfertilization (dpf) zebrafish embryos injected with *c7orf43* MO and probed with C7orf43 and β-actin antibodies. Representative results from two independent experiments are shown. *E*, panels show representative brightfield images of zebrafish embryos treated as in *D* from three or four independent experiments. Rescued embryos (*right*) were co-injected with both *c7orf43* MO and human *C7ORF43* RNA (hC7orf43). *F–H*, top, immunostaining of ciliated organs from 2-dpf embryos treated as in *D* showing ciliation. *White arrowheads*, neuromasts cilia. *Bottom*, quantification of organs with abnormal cilia in 2-dpf embryos. $n >$ 14 olfactory vesicles; $n > 27$ neuromasts; $n > 10$ olfactory placodes. Note that ciliation was rescued upon injection of human C7orf43 mRNA, validating MO specificity. Two-tailed, unpaired Student's *t* test was used. Means ± S.E. are shown from three or four independent experiments. **, $p < 0.01$.

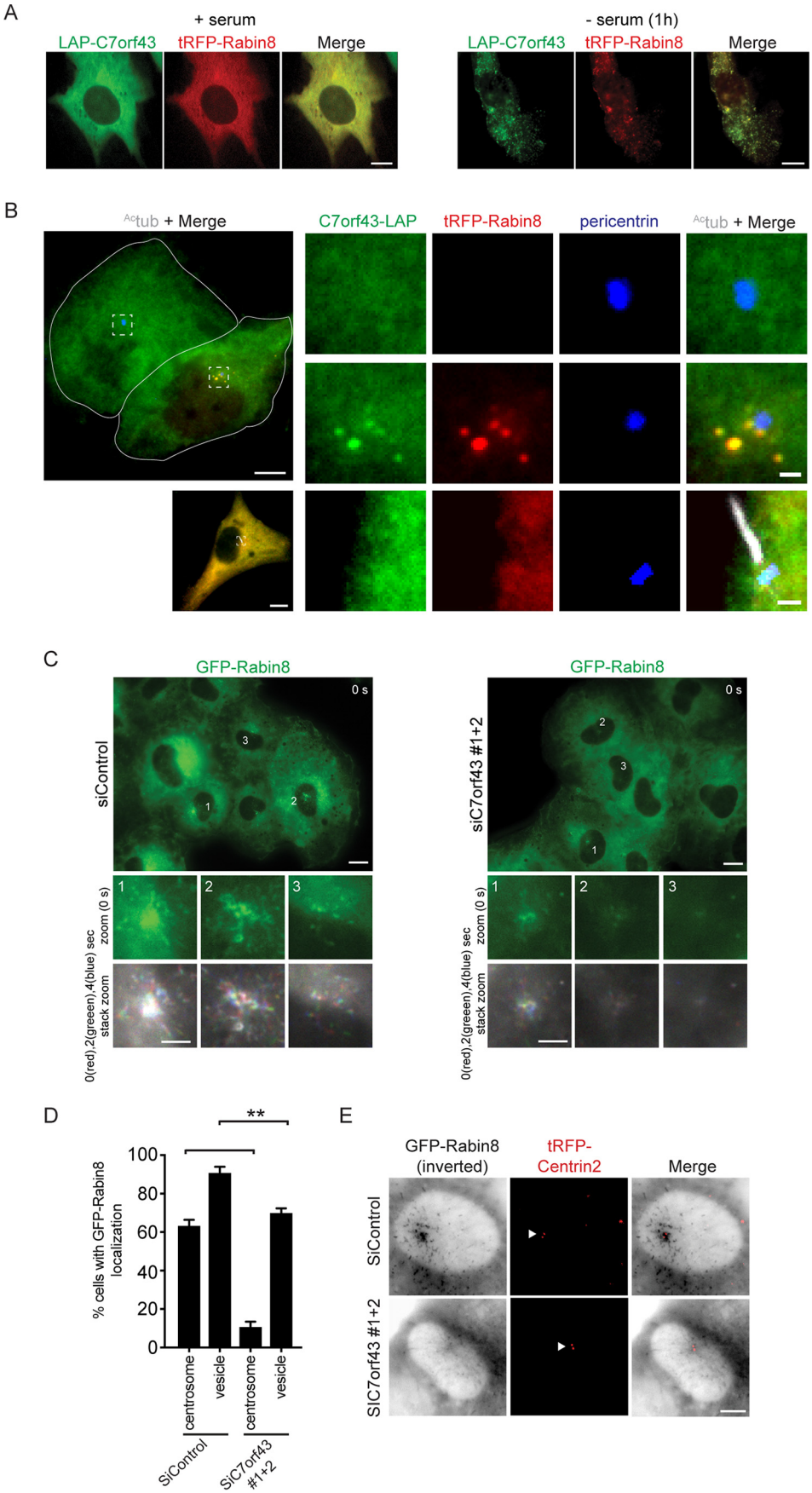
A
+ serum
LAP-C7orf43
tRFP-Rabin8
Merge
- serum (1h)
LAP-C7orf43
tRFP-Rabin8
Merge
B
Actub + Merge
C7orf43-LAP
tRFP-Rabin8
pericentrin
Actub + Merge
C
GFP-Rabin8
0 s
siControl
siC7orf43 #1+2
zoom (0 s)
0(red),2(greeen),4(blue) sec stack zoom
D
**
% cells with GFP-Rabin8 localization
100
80
60
40
20
0
centrosome
vesicle
centrosome
vesicle
SiControl
SiC7orf43 #1+2
E
GFP-Rabin8 (inverted)
tRFP-Centrin2
Merge
SiControl
SIC7orf43 #1+2

(Fig. 5, *B* and *C*). It is not known why C7orf43/TRAPPC14 peptides were not enriched in our MS studies of LAP-TRAPPC10; however, this protein was specifically detected by immunoblotting (Fig. 5*B*).

C7orf43/TRAPPC14 protein expression depends on TRAPPII complex proteins and is required for Rabin8 association with this complex

Given the requirement of TRAPPC14 for preciliary vesicle trafficking of Rabin8 and that TRAPPC14 directly binds to Rabin8 and TRAPPC proteins, we reasoned that it might affect the association between Rabin8 and the TRAPPII complex. Indeed, immunoprecipitated Rabin8 showed an almost complete absence of TRAPPC3, -C4, -C9, and -C10 when TRAPPC14 was depleted (Fig. 6*A*), indicating that TRAPPC14 mediates Rabin8 association with the TRAPPII complex. To determine whether other TRAPPII-specific components affected Rabin8 association with the TRAPPII complex, we knocked down TRAPPC9 or TRAPPC10 using previously described siRNAs and showed similar effects on Rabin8-TRAPPC protein binding, including a loss of TRAPPC14 under these conditions. However, examination of TRAPPC14 expression levels in cell lysates showed that TRAPPC9 and -C10 siRNA treatments strongly reduced TRAPPC14 protein levels but did not affect TRAPPC3 and TRAPPC4 protein expression (Fig. 6*A* and Fig. S6*A*); nor did RNAi depletion of the TRAPPC3 protein affect TRAPPC14 or other TRAPPII-specific components expression (Fig. S6*A*). TRAPPC9 protein levels were also dependent on TRAPPC10 (Fig. 6*A*), whereas TRAPPC14 did not affect other TRAPPII complex subunit expressions. Together, these results indicate that TRAPPC14 expression depends on TRAPPC9 and -C10. Because TRAPPC9 and -C10 affect TRAPPC14 levels, we could not make a conclusion about the requirements for these proteins in Rabin8 interactions with TRAPPC14. To address this question, we transiently expressed TRAPPC14-LAP in HEK293 cells and performed immunoprecipitation experiments in the presence and absence of TRAPPC10 (Fig. 6*B*). Interestingly, TRAPPC14-LAP expression, but not exogenously expressed GFP (Fig. S6*B*), was reduced in cells lacking TRAPPC10, consistent with this TRAPPII complex subunit stabilizing TRAPPC14 protein levels. By using appropriate levels of anti-GFP beads resulting in similar amounts of TRAPPC14-LAP immunoprecipitated in control and TRAPPC10 RNAi treated cells, we could show that TRAPPC10 is dispensable for TRAPPC14-Rabin8 interaction (Fig. 6*B*). We next examined whether TRAPPC14 could associate with the core TRAPP complex in the absence of TRAPPC10. Strikingly, TRAPPC14-LAP failed to interact with the remaining TRAPPC9 proteins and the core TRAPPC proteins TRAPPC2, -C3, and -C4 under these conditions (Fig. 6*B*). Together, these results demonstrate that TRAPPC14 mediates Rabin8 association with the TRAPPII complex, and TRAPPC14 binding to the TRAPPII complex requires TRAPPC10. To demonstrate further that TRAPPC14 can act as a link between Rabin8 and the TRAPPII complex, we examined the association between Rabin8-LAP and FLAG-TRAPPC10 in the presence and absence of overexpressed HA-TRAPPC14. HA-TRAPPC14 increased the pulldown of FLAG-TRAPPC10 with Rabin8-LAP, but not with a negative control FLAG-Rab11a S25N (Fig. 6*C*) (7, 9). Together, these results and the observation that TRAPPC14 expression is affected by TRAPPC9 and -C10 and directly interacts with TRAPPC10 suggest that TRAPPC14 is a TRAPPII-specific protein and mediates this complex's association with Rabin8 needed for its preciliary trafficking to the centrosome.

C7orf43/TRAPPC14 interacts with DAP components, and DAPs are required for Rabin8 vesicular accumulation at the centrosome

Impaired Rabin8 centrosomal accumulation caused by TRAPPC14 knockdown suggested that TRAPPC14 may have a role in tethering GFP-Rabin8 preciliary vesicles at the MC. Previous studies have identified CEP164 as a DAP component that interacts with Rabin8 and is required for membrane docking to the MC (20). Thus, we investigated whether CEP164 is important for preciliary vesicular trafficking and discovered that GFP-Rabin8 centrosomal accumulation was not affected by CEP164 RNAi (Fig. 7*A* and Fig. S7*A*). CEP83 sits upstream in DAP assembly at the MC and is needed for CEP164 and FBF1 localization to the DAPs (46). Thus, we investigated whether depletion of CEP83 affected GFP-Rabin8 centrosomal accumulation. Strikingly, knockdown of CEP83 severely diminished GFP-Rabin8 centrosomal accumulation (Fig. 7*A* and Fig. S7*A*). Because FBF1 is downstream of CEP83 and has been shown to be required for ciliogenesis in RPE-1 cells (46, 47), we next investigated whether FBF1 affects GFP-Rabin8 trafficking. As was observed with CEP83 RNAi, FBF1 depletion similarly prevented GFP-Rabin8 centrosomal accumulation (Fig. 7*A* and Fig. S7*A*). Based on these results, we examined TRAPPC14

Figure 3. C7orf43 is required for Rabin8 preciliary trafficking to the centrosome. *A*, live-cell imaging using spinning-disk confocal microscopy of 24-h transiently co-expressed LAP-C7orf43 and tRFP-Rabin8 in RPE-1 cells grown in the presence of serum or serum-starved for 1 h. Representative images are shown from three independent experiments. *Scale bars*, 5 μm. *B*, RPE-1 cells transiently expressing C7orf43-LAP and tRFP-Rabin8 for 24 h and serum-starved the last hour, fixed and stained with antibodies marking the centrosome (pericentrin) and ^{Ac}tub (cilia). *Merged* refers to *green*, *red*, and *blue* channels. The *white dashed boxes* in the *left panels* show the full cell corresponding to *magnified panels* to the *right*. The *top left image* displays a *white outline* of two cells, one with (*top cell* for magnified images in the *top right panels*) and the other without (*bottom cell* for *magnified images* in the *middle right panels*) tRFP-Rabin8 expression. The *bottom* left image displays a cell with a cilia (magnified images in the *bottom* right panels) expressing C7orf43-LAP and tRFP-Rabin8. Representative images are shown from three independent experiments. *Scale bars*, 5 μm (*left image*) and 0.5 μm (*magnified right images*). *C*, representative images from time lapses of RPE-1 GFP-Rabin8 cells treated with either siControl (*left panels*) or siC7orf43 (*right panels*), serum-starved for 1–2 h and imaged by live epifluorescence microscopy from three independent experiments. *Scale bar*, 10 μm. *Top insets*, *zoom* of GFP-Rabin8 centrosomal accumulation in cells 1, 2, and 3 at time point 0 s. *Bottom insets*, to better visualize vesicle movement, zoom images of *insets* from time points 0, 2, and 4 s were *pseudocolored red* (0 s), *green* (2 s), and *blue* (4 s), respectively, and merged. *Scale bars*, 5 μm. *D*, corresponding quantification of GFP-Rabin8 centrosomal and vesicular accumulation from *C*. Two-tailed, unpaired Student's *t* test was used. Means ± S.E. (*error bars*) are shown from three independent experiments with $n > 150$ cells quantified in total. **, $p < 0.01$; ***, $p < 0.001$. *E*, representative images of live RPE-1 cells stably expressing GFP-Rabin8 and tRFP-CENTRIN2, treated with either siControl or siC7orf43, serum-starved at 72 h post-transfection for 2 h to promote Rabin8 trafficking, and imaged by epifluorescence microscopy from three independent experiments. GFP-Rabin8 signal was inverted to better visualize membrane vesicles. *White arrow*, tRFP-CENTRIN2 localizing to mother and daughter centrioles. *Scale bar*, 5 μm.

interactions with CEP83 and FBF1. Remarkably, we showed that HA-TRAPPC14, but not control HA-luciferase, immunoprecipitated strongly with LAP-FBF1 (Fig. 7*B*) and, to a lesser extent, with LAP-CEP83 (Fig. S7*B*). Together, our findings suggest a model whereby TRAPPC14 performs a dual function of mediating Rabin8 association with the TRAPPII complex and helps tether GFP-Rabin8 preciliary vesicles to the DAPs on the MC (Fig. 7*C*).

A

	LAP		C7orf43-LAP	
Protein	PSM	%C	PSM	%C
C7orf43	0	0	422	37.4
GFP	1409	60.5	297	60.5
TRAPPC9	1	2.7	26	12.8
TRAPPC10	0	0	26	12.2
TRAPPC2	0	0	4	18.6
TRAPPC6B	0	0	4	24.6
TRAPPC3	0	0	4	17.2
TRAPPC4	0	0	4	22.8
TRAPPC2L	0	0	4	11.9
TRAPPC5	0	0	2	11.7
TRAPPC6A	0	0	0	0
Rabin8	0	0	0	0
TRAPPC8	1	1.2	1	1.3
TRAPPC11	0	0	0	0
TRAPPC12	0	0	0	0
TRAPPC13	0	0	0	0

B

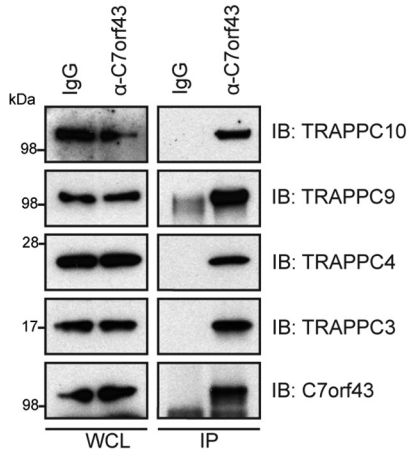

C

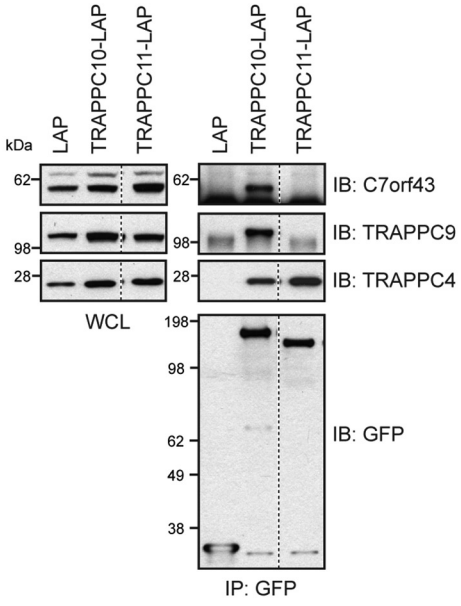

D

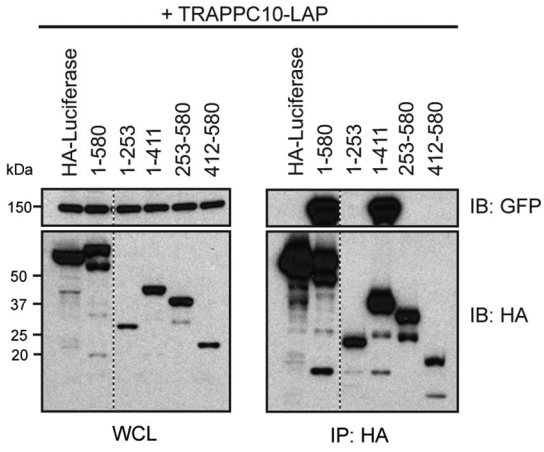

E

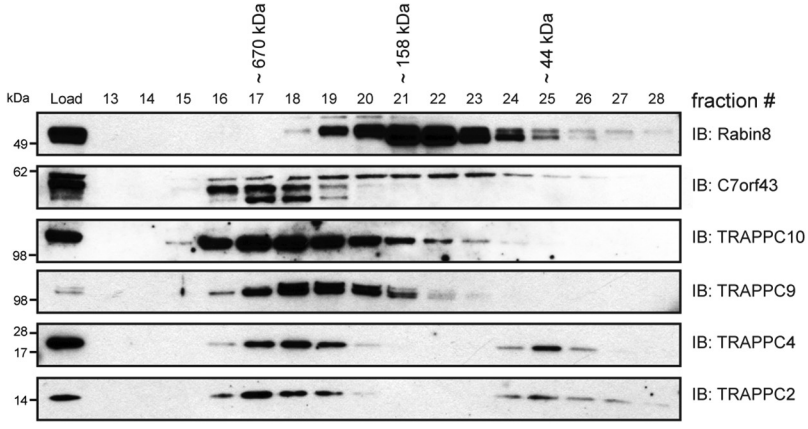

F

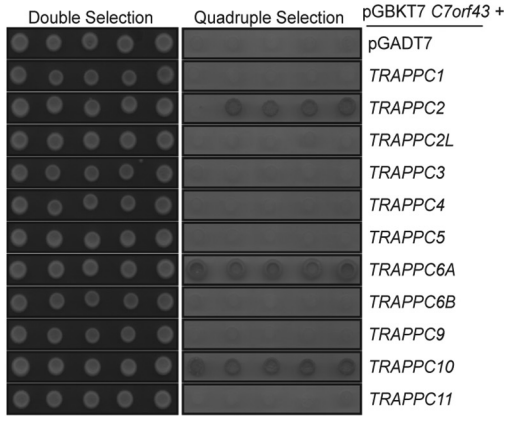

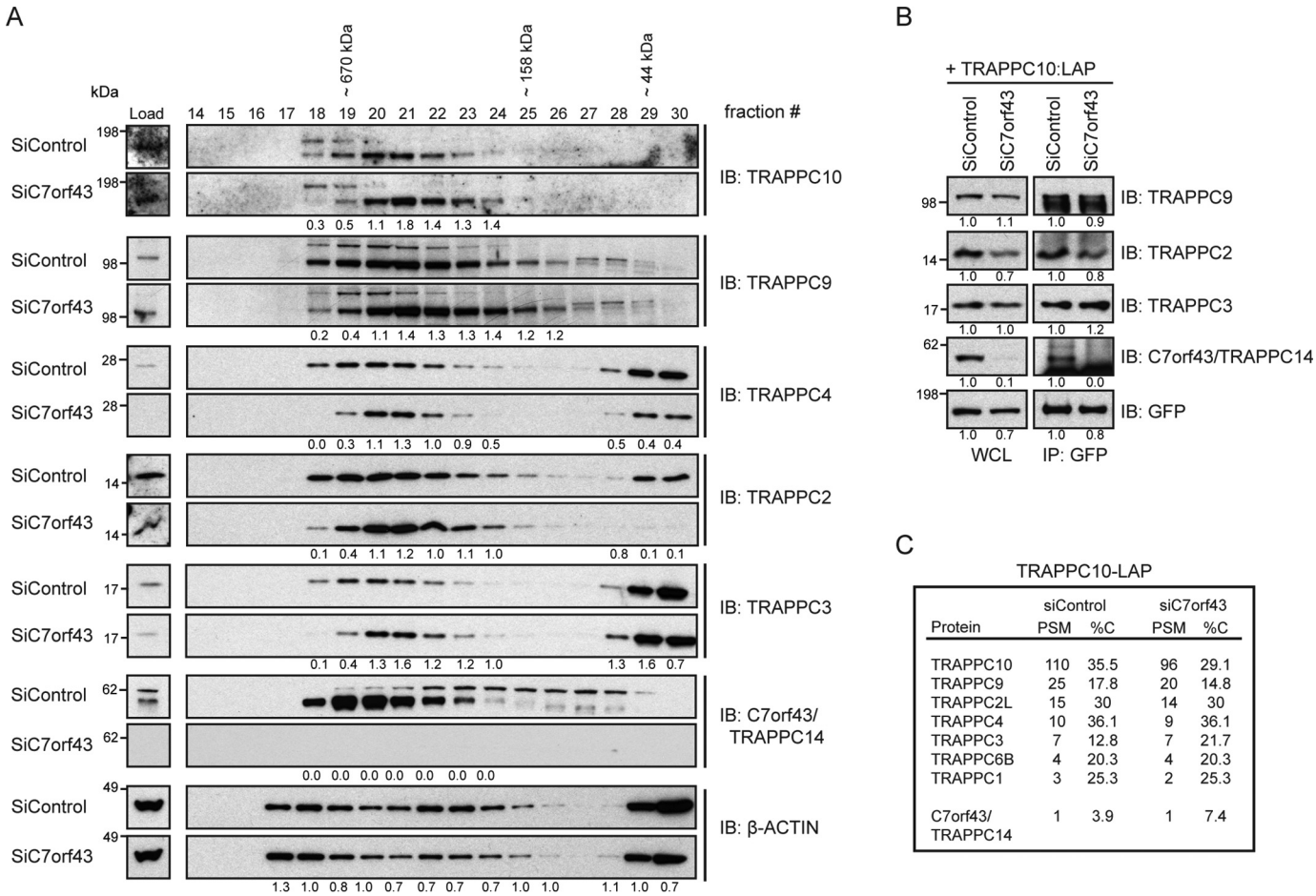

Protein	siControl PSM	siControl %C	siC7orf43 PSM	siC7orf43 %C
TRAPPC10	110	35.5	96	29.1
TRAPPC9	25	17.8	20	14.8
TRAPPC2L	15	30	14	30
TRAPPC4	10	36.1	9	36.1
TRAPPC3	7	12.8	7	21.7
TRAPPC6B	4	20.3	4	20.3
TRAPPC1	3	25.3	2	25.3
C7orf43/ TRAPPC14	1	3.9	1	7.4

Figure 5. C7orf43 is a TRAPPII complex component but is not required for the core complex integrity. *A*, immunoblotting of size-exclusion chromatography fractions performed using lysate from either siControl or siC7orf43(#1+#2)–treated HEK293 cells. Blots were probed with antibodies against C7orf43/TRAPPC14, TRAPPC proteins, and actin. Comparative protein ratios of siC7orf43/siControl were determined by densitometry and are shown *below* blots for expressing fractions. Representative results from two independent experiments are shown. *B*, immunoprecipitation analysis of transiently expressed TRAPPC10-LAP after siControl and siC7orf43/TRAPPC14(#1+#2) treatments in HEK293 cells. Blots were probed with antibodies against GFP and TRAPPC proteins. Protein levels compared with siControl in WCL and immunoprecipitations (*IP*) were determined by densitometry analysis and are shown *below* blots normalized for differences in GFP expression between RNAi treatments. Representative results from two independent experiments are shown. *C*, PSM and %C from MS analysis of immunoprecipitated TRAPPC10-LAP from transient expression in HEK293 cells after treatment with siControl or siC7orf43(#1+#2) for 72 h from a single experiment.

Discussion

In our present study, we have identified an uncharacterized TRAPPII-specific component, C7orf43/TRAPPC14, that regulates Rabin8 preciliary trafficking and ciliogenesis. We demonstrate that TRAPPC14 directly binds to core TRAPP, TRAPPII-specific subunits, and Rabin8 and is required for TRAPPII complex association with Rabin8. TRAPPC14 interaction with this TRAPP complex depends on TRAPPII-specific subunits, and we show that TRAPPC14 is not important for the integrity of the TRAPPII complex; however, TRAPPII-specific proteins are necessary for TRAPPC14 protein expression. Finally, we discovered that TRAPPC14 can interact with the DAP proteins FBF1 and CEP83 and that ablation of these DAPs inhibits Rabin8 accumulation at the centrosome. Together, our work suggests that during ciliogenesis, TRAPPC14 functions to link Rabin8 to the TRAPPII complex and is involved in tethering Rabin8 preciliary vesicles to DAPs at the MC, upstream of cilium assembly.

Biochemical, localization, and ciliogenic studies indicated that TRAPPC14 is associated with the TRAPPII complex. In addition to the specific interactions between TRAPPC10 and TRAPPC14, we show that the expression of TRAPPC14 depends on TRAPPC9 and -C10, but not the core TRAPPC3, as

Figure 4. C7orf43 specifically associates with the TRAPPII complex. *A*, PSM and percent coverage (%*C*) values from MS analysis of C7orf43-binding proteins immunoprecipitated with a GFP antibody from HEK293 cells transiently expressing either LAP alone or C7orf43-LAP from a single experiment. *B*, immunoblot (*IB*) showing immunoprecipitation of endogenous C7orf43 from HEK293 cells with either IgG control or C7orf43 antibody. The blot was probed with antibodies against TRAPPC proteins as indicated on the *right*. Representative results from two independent experiments are shown. *C*, immunoprecipitation of LAP-tagged proteins from HEK293 cells transfected with LAP, TRAPPC10-LAP, or TRAPPC11-LAP is shown. GFP, C7orf43, TRAPPC9, and TRAPPC4 antibodies were used for immunoblotting. Representative results from two independent experiments are shown. *D*, domain mapping of HA-C7orf43 for TRAPPC10-LAP binding as performed in Fig. 1*D*. A representative blot from three independent experiments is shown. *E*, immunoblotting of size-exclusion chromatography on HEK293 cell lysate using Rabin8, C7orf43, and TRAPPC antibodies. Representative results from three independent experiments are shown. *F*, yeast two-hybrid analysis of the GAL4 DNA-binding domain (*BD*) fused to C7orf43 co-transformed with GAL4 activating domain (*AD*) control or TRAPPC fusions. Control double selection (leucine and tryptophan) and quadruple selection (leucine, tryptophan, histidine, and adenine) are shown. Five independent colonies are shown, and the results are representative from two or three independent experiments.

the TRAPPII-specific components likely stabilize TRAPPC14 protein levels by mediating its association with the complex. TRAPPC14 is highly conserved in mammals and more distant invertebrates (Figs. S2 and S3), and, interestingly, TRAPPC14 has some homology to the yeast TRAPPII protein Trs65 (Fig. S5), which has been proposed to be C5orf44/TRAPPC13 in mammalian cells, despite Trs65 having been linked to TRAPPII functions in yeast (31, 48–50). Given our observations that TRAPPC14 is associated with the TRAPPII complex and has a similar molecular weight and some sequence homology, it is

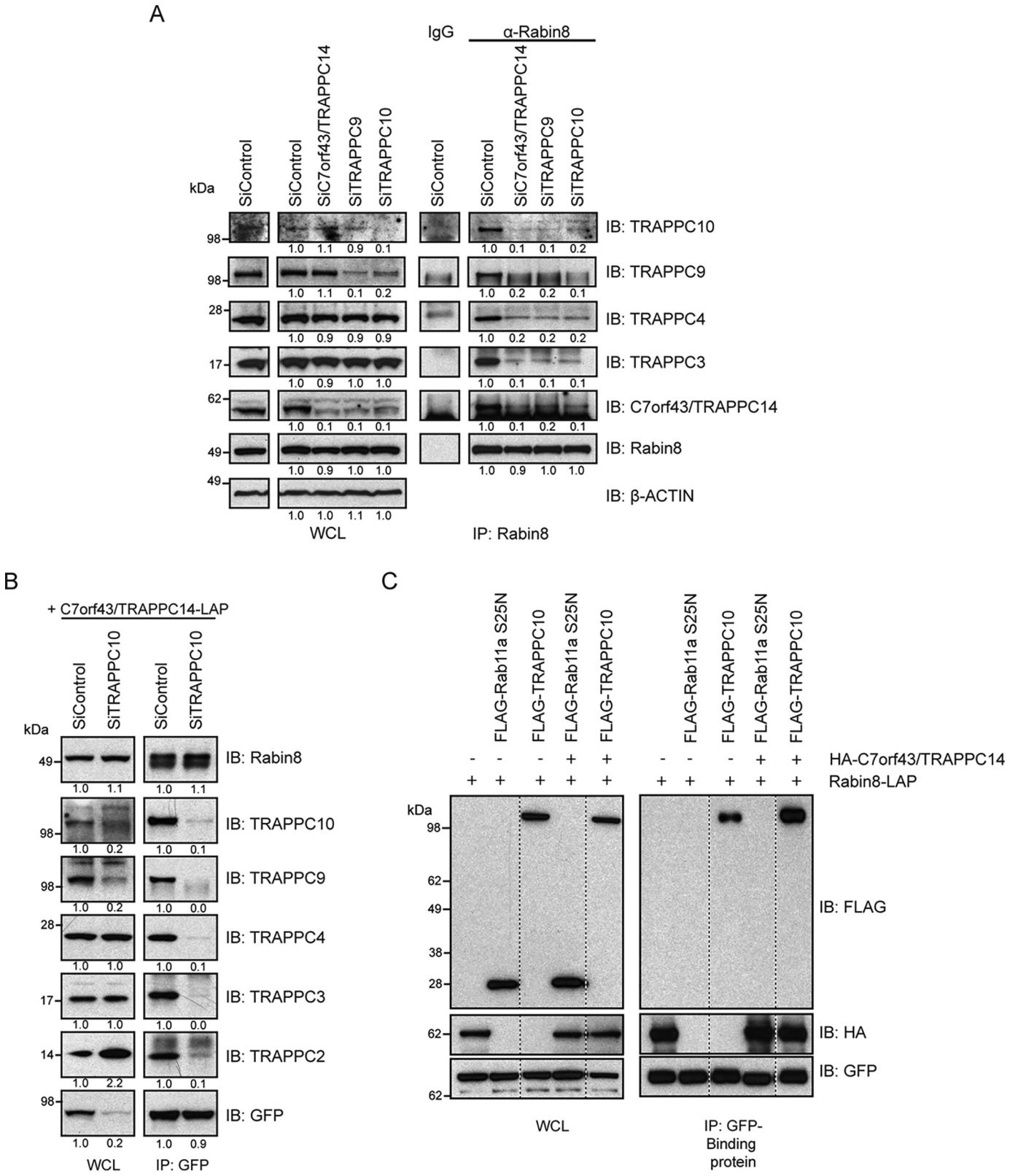

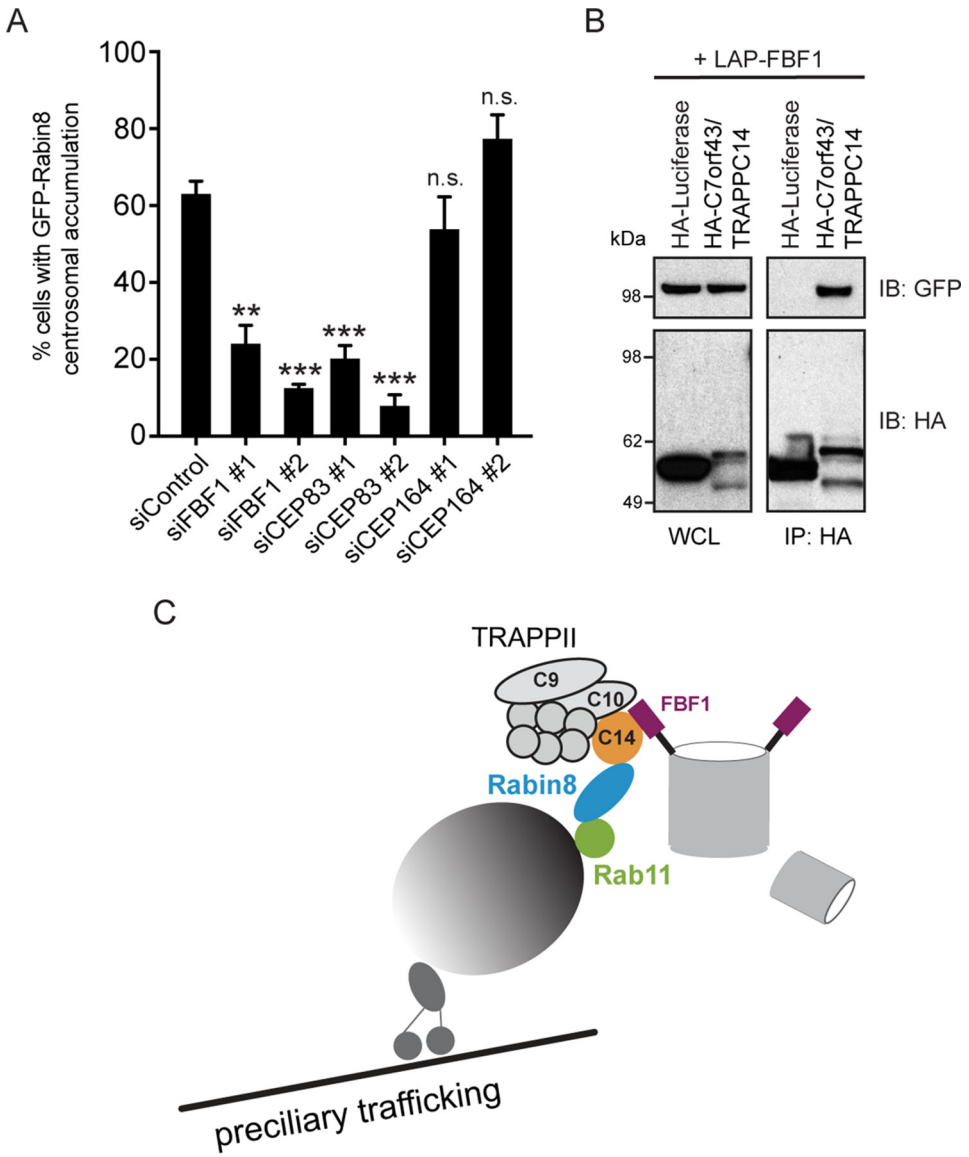

Figure 7. Distal appendage proteins FBF1 and CEP83 are required for GFP-Rabin8 centrosomal accumulation and bind to TRAPPC14. *A*, plot showing quantification of GFP-Rabin8 centrosomal accumulation as described in Fig. 3*D* in GFP-Rabin8–expressing RPE-1 cells treated with siRNA against DAP proteins. Two-tailed, unpaired Student's *t* test was used. Means ± S.E. (*error bars*) are shown from three independent experiments with $n > 150$ cells in total. **, $p < 0.01$; ***, $p < 0.001$; *n.s.*, not significant. *B*, immunoblotting of immunoprecipitated HA-luciferase or HA-TRAPPC14 with LAP-FBF1. Representative results from three independent FBF1 experiments performed in HEK293 are shown. *C*, model for TRAPPII complex and TRAPPC14 mediating vesicular Rabin8 delivery to MC for primary cilium formation.

conceivable that this protein is the orthologue of Trs65. Consistent with this idea, Trs65 and TRAPPC14 are dispensable for TRAPPII complex integrity (31) (Fig. 5, *A–C*), although Trs65 was shown to function in complex oligomerization, which does not appear to be the case with TRAPPC14. The shift to a smaller TRAPPII complex seen after TRAPPC14 depletion is likely associated with loss of TRAPPC14, and possibly other proteins, associated with this complex (Fig. 5*A*). Experimental conditions used in these studies may explain differences in oligomerization requirements between Trs65 and TRAPPC14 (31), and, notably, the importance of Trs65 in TRAPPII oligomerization is unclear as yeast are viable without the protein (49), whereas the other TRAPPII complex–specific components Trs120 and Trs130 are essential (51, 52). Trs65 has also been shown to

Figure 6. TRAPPC14 mediates interaction between Rabin8 and the TRAPPII complex. *A*, immunoblot (*IB*) showing immunoprecipitation of endogenous Rabin8 from HEK293 cells after treatment with either control, TRAPPC9, TRAPPC10, or TRAPPC14 siRNA for 72 h. Immunoblots were probed with antibodies as indicated on the *right*. Protein levels compared with siControl treatments were determined by densitometry analysis and are shown *below* blots normalized for protein level differences in actin for WCL and Rabin8 for immunoprecipitations (*IP*). Representative results from three independent experiments are shown. *B*, immunoprecipitation analysis of transiently expressed TRAPPC14-LAP after siControl and siTRAPPC10 treatments as described in *A*. TRAPPC14-LAP was transfected into cells 24 h after RNAi treatment. Immunoblots were probed with antibodies as indicated. Protein levels compared with siControl treatments were determined by densitometry analysis and are shown *below* blots normalized for protein level differences in Rabin8, TRAPPC3, and TRAPPC4 for WCL and GFP for immunoprecipitations. Representative results from three independent experiments are shown. *C*, immunoblot for co-expression and co-immunoprecipitation of Rabin8-LAP with FLAG-TRAPPC10 or FLAG-Rab11aS25N with and without HA-TRAPPC14 from HEK293 cells. Immunoblots were probed with GFP, HA, and FLAG antibodies. Representative results from three independent experiments are shown.

bind to the Arf1p exchange factor, suggesting a role in COPI vesicle tethering (53), which is consistent with a tethering function for TRAPPC14 in preciliary trafficking. However, as the TRAPPIII complex proteins TRAPPC11 and -C12 do not appear to have yeast orthologues (34), it would also not be surprising if TRAPPC14 was not conserved in yeast, especially given the absence of cilia in this organism. Thus, our finding that TRAPPC14 and other TRAPPII complex proteins are needed for ciliogenesis could indicate a distinct function in ciliated organisms, and proteins such as TRAPPC14 may be important for these specifications. Interestingly, TRAPPC9, TRAPPC10, and C7orf43 were shown by MS analysis to interact with AMOTL2, an inhibitor of Wnt signaling, which, in hypoxic conditions and tumors, was proposed to negatively regulate trafficking of polarity proteins by binding and inactivating the TRAPPII complex (54). C7orf43/TRAPPC14 was not investigated in this study, but these results present another example in which the TRAPPII-specific module, possibly through TRAPPC14, could regulate complex activity.

Recently, a mutation in C7orf43 was identified in a patient with autosomal recessive primary microcephaly (MCPH) (55), and mutations in TRAPPC9 (56) and TRAPPC10 (57) as well as core TRAPPC proteins TRAPPC2L, -C6A, and -C6B have also been identified in patients displaying autosomal recessive intellectual disabilities, including MCPH or other brain abnormalities (22). This C7orf43-truncating homozygous mutation resulting in a C7orf43$_{1-205}$ fragment based on our results, is expected to lack the ability to associate with TRAPPC10 (Fig. 4*D*). These clinical observations are consistent with our conclusion that C7orf43 is a component of the TRAPPII complex. In this paper (55), C7orf43 was referred to as MAP11, as it associates with mitotic spindles and α-tubulin in SH-SY5Y neuroblastoma cells, and knockdown of this protein affected cell viability and reduced proliferation. In RPE-1 and NeoHDF cells, we only observed a small effect on cell numbers following knockdown (Fig. 2, *B* and *C*). Consistent with our results, C7orf43 was localized to vesicles in SH-SY5Y cells (55). Importantly, neurogenesis defects in microcephaly have been attributed to mutations in genes that contribute to centrosome biogenesis and cilia stability, in turn, impinging on ciliary signaling pathways controlling cell patterning, proliferation, and survival during development (23–26, 58). Thus, based on these observations, investigation of connections between the TRAPPII complex and MCPH and ciliopathies is merited.

Our findings that knockdown of TRAPPC14 and the DAPs CEP83 and FBF1 impair Rabin8 preciliary vesicle accumulation at the centrosome present an intriguing possibility that the TRAPPII complex participates in tethering preciliary vesicles to the MC, possibly upstream of vesicular docking mediated by CEP164. CEP164 interacts with Rabin8, and our observation that Rabin8 can still accumulate in the centrosomal region after CEP164 depletion is in agreement with previous studies showing that undocked vesicles are in proximity to the MC in cells lacking CEP164 but fail to dock to the MC DAPs (20, 59). Loss of GFP-Rabin8 enrichment at the centrosome after DAP or TRAPPC14 ablation would be expected to affect downstream Rab8 activation needed for ciliogenesis (5). Interestingly, FBF1 has been recently shown to localize to the outermost region between adjacent DAP blades, known as the DAP matrix, and is positioned proximal to the ciliary membrane in mature cilia (47), conceivably allowing for interaction with vesicles trafficked to the MC. Rabin8 function during ciliogenesis requires another large vesicle trafficking/tethering complex, the exocyst (14, 15). The exocyst component Sec15 binds Rabin8 to assist with Rab8 activation. Together, these observations and our work indicate that large-molecular weight complexes play key roles in coordinating membrane docking and assembly events at the MC during ciliogenesis. Given that the Rab11-Rab8 cascade has also been shown to be important in apical plasma membrane formation in polarized epithelial cells (16) and has been implicated in immune synapse transport (17), it will be interesting to examine requirements for TRAPPC14 and the TRAPPII complex in these processes. Like the TRAPPII complex, the Rab11-Rab8 cascade is conserved from yeast to humans (18), although it is not known whether the yeast TRAPPII complex interacts directly with Sec2 to help mediate bud neck formation.

Given that the TRAPPII complex can function as a GEF for yeast and fly orthologs of Rab11 (37, 38), it is conceivable that TRAPPC14 could affect Rab11 GTPase activity, which could also explain why GFP-Rabin8 failed to localize to the centrosome following TRAPPC14 ablation. However, it has been shown that the TRAPPII complex does not have GEF activity toward Rab11 in mammalian cells (39), although it is not known whether TRAPPC14 was present in reported purified complexes. Moreover, a recombinant TRAPPII complex comprised of the core, TRAPPC9, and TRAPPC10 that was purified from *Drosophila* was sufficient for GEF activity toward Rab1 and Rab11 (38), which further suggests that TRAPPC14 is dispensable for GEF functioning. Consistent with this theory, GFP-Rabin8 vesicular trafficking, although diminished, was still observed following depletion of TRAPPC14, suggesting that Rab11 GTPase activity was not affected in our studies. The TRAPPII complex has also been shown to be a GEF for Rab18, important for lipid droplet homeostasis (60), which could also involve TRAPPC14 function.

In summary, our present work reveals how the TRAPPII complex functions in Rabin8 preciliary trafficking and ciliogenesis and identifies a previously uncharacterized TRAPPII-specific component in C7orf43/TRAPPC14. Importantly, our work supports other reported findings that the TRAPPII complex functions as a membrane tether (29, 40, 41, 53), although in this case between membrane vesicles and the mother centriole DAPs.

Experimental procedures

Plasmids, reagents, and yeast two-hybrid analysis

Coding sequences for C7orf43 (NM_018275.5), TRAPPC1 (BC032717), TRAPPC2 (BC052618), TRAPPC2L (BC011369), TRAPPC3 (NM_001139444), TRAPPC4 (BC010866), TRAPPC5 (HQ257952), TRAPPC6A (BC004450), TRAPPC6B (BC047328), TRAPPC9 (NM_031466), TRAPPC10 (NM_003274.5), and TRAPPC11 (NM_021942.6) were purchased in pENTR plasmids from DNASU Plasmid Repository (Tempe, AZ) and subcloned into Gateway destination vectors. FBF1 (BC023549.2) was cloned into pDONR201 following PCR

amplification with Phusion polymerase (Catalog no. M0530L, NEB) using a cDNA plasmid purchased from Transomic Technologies (FMG). CEP83 (NP_001035858.1) coding sequence was amplified by PCR from an RPE-1 cDNA library. C7orf43-truncated constructs (1–253, 1–411, 253–580, 412–580) were generated by PCR, cloned into pDONR201 plasmids, and inserted into the pCS2+-HA destination vector as described (9). All PCR amplified constructs were sequence verified. GFP-Rabin8 full length and truncations and GFP-Rab11a Q70L and S25N were previously described (9). gLAP1 and/or gLAP7 (61) vectors were used to generate NH2- and COOH-fusions of C7orf43, TRAPPC10, and TRAPPC11. pEGFP-CI empty vector was used to express GFP alone. For recombinant protein expression, full-length Rabin8 and C7orf43 were subcloned from the donor vectors into the bacteria expression vectors pDEST-15 (ThermoFisher) and pDEST-527 (Protein Expression Laboratory, Frederick National Lab for Cancer Research) to express GST or 6×His tagged proteins. The empty vector pGEX-4T-1 was used to express the GST protein. Rab11a S25N and TRAPPC10 were cloned into Gateway vector pDEST-305 (Protein Expression Laboratory, Frederick National Lab for Cancer Research) to create a pPGK-driven, Flag (3×), N-terminus-tagged fusion protein. TRAPPC cDNA in pDONR201 were used to generate pGADT7 expression plasmids using Gateway cloning. Restriction-digested, PCR-amplified C7orf43 was ligated in pGBKT7 and sequenced. Yeast two-hybrid was performed as previously described (62). X-tremeGENE 9 (Roche) was used for DNA transfections into cells according to manufacturer's instructions. For knockdown experiments, cells were transfected with siRNA duplexes obtained from Dharmacon (Table S1) using RNAiMAX (Invitrogen). Complete protease inhibitors (Catalog no. 4693132001, Roche/Millipore Sigma) and PhosSTOP phosphatase inhibitor (Catalog no. 4906845001, Roche/Millipore Sigma).

Antibodies

Antibodies were used for C7orf43 (Abnova catalogue no. PAB21203 and Novus catalogue no. NBP1-83808), acetylated α-tubulin (^{Ac}tub) (catalogue no. T7451, Sigma), pericentrin (catalogue no. NB100-61071, Novus), GFP for immunoprecipitation (custom; rabbit polyclonal), GFP-HRP (catalogue no. 130-091-833, Miltenyi Biotec), FLAG-HRP (catalogue no. A8592, Sigma-Aldrich), HA-HRP (catalogue no. 12013819001, Roche Applied Science/Sigma), β-actin-HRP (catalogue no. A3854, Sigma-Aldrich), Rab3IP/Rabin8 (rabbit) (catalogue no. 12321-1-AP, Proteintech), Rab3IP/Rabin8 (mouse/clone OTI4A7) (catalogue no. TA808962, Origene), GM130 (catalogue no. 610823, BD Biosciences), myosin-Va (catalogue no. NBP1-92156, Novus), CEP83/CCDC41 (catalogue no. 26013-1-AP, Proteintech), CEP164 (catalogue no. 22227-1-AP, Proteintech), FBF1 (catalogue no. 11531-1-AP, Proteintech), TRAPPC9 (catalogue no. 16014-1-AP, Proteintech), TRAPPC2 (catalogue no. 12484-1-AP, Proteintech), TRAPPC3 (catalogue no. 15555-1-AP, Proteintech), TRAPPC4 (catalogue no. AB57364, Abcam), GST-HRP (catalogue no. HRP-66001, Proteintech), and TRAPPC10/TMEM1 (catalogue no. AB58247, Abcam). Secondary antibodies used were DyLight 405 anti-mouse (catalogue no. 715-475-151, Jackson ImmunoResearch), DyLight 405 anti-rabbit (catalogue no. 715-475-152, Jackson ImmunoResearch), Alexa 568 anti-rabbit (catalogue no. A10042, Thermo Fisher Scientific), Alexa 647 anti-rabbit (catalogue no. A31573, Thermo Fisher Scientific), and Alexa 647 anti-mouse (catalogue no. A31571, Thermo Fisher Scientific).

Cell lines and cell line generation

NeoHDF, RPE-1, HEK293, and 293T cells were obtained from ATCC. RPE-1 Flp-In were a kind gift from Peter Jackson (Stanford University, Palo Alto, CA). RPE-1 GFP-Rabin8 and RPE-1 GFP-Rabin8 + tRFP-Centrin2 cells were described previously (9). RPE-1 Flp-In LAP-Rabin8 cells were generated as described previously (11).

Purification and mass spectrometry

Tandem affinity purification and MS analysis for LAP-Rabin8 in the RPE-1 Flp-In and LAP-Rabin8$_{1-142}$ 293Trex Flp-In cells were performed as described previously (9). For the remaining MS analysis, each 15-cm dish of HEK293 cells was grown to a confluence of 40% and transiently transfected with either LAP alone, TRAPPC10-LAP, or C7orf43-LAP. After 24–48 h, cells were lysed on ice in LAP300 buffer (50 mM HEPES, pH 7.4, 300 mM KCl, 1 mM EGTA, 1 mM $MgCl_2$, 10% glycerol, 0.5 mM DTT, protease inhibitors (Roche Applied Science), PhosSTOP (Roche Applied Science), and 0.1% NP-40) followed by immunoprecipitation for 1 h with Protein A beads conjugated with GFP antibody. Beads were washed with lysis buffer, resuspended in 25 mM NH_4HCO_3, pH 8.4, and frozen in liquid nitrogen for subsequent on-bead trypsin digestion to extract the peptides. Tryptic digests were fractionated using strong cation-exchange LC and performed as described previously (63).

For MS acquisition and data analysis, the dried peptide fractions were reconstituted in 0.1% TFA and subjected to nanoflow LC (Thermo Easy nLC 1000, Thermo Scientific) coupled to high-resolution tandem MS (Q Exactive, HF, Thermo Scientific). MS scans were performed in the Orbitrap analyzer at a resolution of 60,000 with an ion accumulation target set at 3e^6 over a mass range of 300–16,500 m/z, followed by MS/MS analysis at a resolution of 15,000 with an ion accumulation target set at 1e^5. MS2 precursor isolation width was set up at 1.4 m/z, normalized collision energy was 30, and charge state 1 and unassigned charge states were excluded. Acquired MS/MS spectra were searched against the human Uniprot protein database along with a contaminant protein database, using SEQUEST and Fixed Value peptide-spectrum match (PSM) validator algorithms in the Proteome Discoverer 1.4 software (Thermo Scientific). The precursor ion tolerance was set at 10 ppm, and the fragment ion tolerance was set at 0.6 Da along with methionine oxidation included as dynamic modification. Only fully tryptic peptides with up to two miscleavages with charge state–dependent cross-correlation Xcorr ≥ 2.1 for $[M + H]^{1+}$, ≥ 2.5 for $[M + 2H]^{2+}$, and ≥ 3.2 for $[M + 3H]^{3+}$ and Δ correlation (ΔC_n) ≥ 0.08 were considered as positive identification.

Immunofluorescence and live-cell microscopy

For immunofluorescence studies, RPE-1 and NeoHDF cells were fixed with 4% paraformaldehyde and stained with antibodies as described (9) and imaged by epifluorescence microscopy using a ×63 oil immersion objective unless otherwise indicated. For ciliation determinations, cells were stained with ^{Ac}tub and pericentrin antibodies, and cilia numbers were determined as described (9). Live-cell epifluorescence imaging of RPE-1 GFP-Rabin8 cells with and without transiently expressed LAP-C7orf43 and RPE-1 GFP-Rabin8 + tRFP-Centrin2 cells was performed at 37 °C and quantified as described (9). Briefly, cells were serum-starved for 1–2 h and imaged live (37 °C, 5% CO_2) every 1 s for 5–10 s using an X-Cite 120 lamp at 50% power and a ×63 1.3 numerical aperture oil objective. Cells with GFP-Rabin8 vesicles in the cytoplasm and centrosome accumulation were counted.

For whole-mount zebrafish studies, embryos were fixed in 4% paraformaldehyde at 48 h postfertilization and stained with anti-^{Ac}tub and secondary Alexa 488–conjugated antibodies, phalloidin conjugated with Alexa 568 (catalogue no. A12380, Molecular Probes Life Technologies), and Hoechst. Ciliated organs from stained embryos were imaged using the Marianas SDC microscope and ×40 1.4 numerical aperture objective and analyzed for ciliation defects as described previously (5).

Immunoprecipitations, immunoblotting, and densitometry

For domain mapping and immunoprecipitations using multiple overexpressed proteins, HEK293 cells were transfected with the indicated constructs. After 48 h of transfection, cells were washed with PBS, lysed in 1% NP-40 lysis buffer (137 mM NaCl, 20 mM Tris, pH 8.0, 10% glycerol, 1% NP-40) supplemented with protease and phosphatase inhibitors followed by immunoprecipitation with Protein A beads conjugated with a custom GFP antibody or magnetic HA beads (catalogue no. 88836, Thermo Fisher Scientific). Lysis buffer was used for washes. Samples were resolved using SDS-PAGE, transferred to nitrocellulose membrane, and probed with antibodies.

For endogenous immunoprecipitations with and without overexpressed proteins, low-salt Triton lysis buffer (30 mM Tris-HCl, pH 8.0, 75 mM NaCl, 10% glycerol, 1% Triton X-100 with 5 mM $MgCl_2$, and protease and phosphatase inhibitors) was used to lyse cells, and a Rab3IP/Rabin8 (rabbit) (catalogue no. 12321-1-AP, Proteintech), C7orf43 (catalogue no. PAB21203, Abnova), or GFP custom antibody was incubated with lysate overnight followed by the addition of Protein A/G magnetic beads and incubation for 3 h. Rab3IP/Rabin8 (mouse/clone OTI4A7) (catalogue no. TA808962, Origene) was used to blot for endogenous Rabin8 after immunoprecipitation using Protein A/G magnetic beads.

For immunoprecipitations combining recombinant proteins and GFP or LAP fusion proteins, radioimmune precipitation assay lysis buffer (20 mM Tris-HCl, pH 8.0, 137 mM NaCl, 10% glycerol, 1% NP-40 alternative, 0.1% SDS, 0.1% sodium deoxycholate with protease inhibitors) was used to lyse cells, and a GFP custom antibody was incubated with lysate overnight at 4 °C followed by the addition of Protein A/G magnetic beads (catalogue no. 88802, Thermo Fisher Scientific) and incubation for 3 h. Beads were washed six times with radioimmune precipitation assay lysis buffer. Recombinant protein and washed beads with attached GFP-fused proteins were incubated in low-salt Triton buffer (30 mM Tris-HCl, pH 8.0, 75 mM NaCl, 10% glycerol, 1% Triton X-100 with 5 mM $MgCl_2$ and protease and phosphatase inhibitors) overnight at 4 °C followed by the addition of Protein A/G magnetic beads and incubation for 3 h. Rab3IP/Rabin8 (mouse/clone OTI4A7) (catalogue no. TA808962, Origene) was used to blot for endogenous Rabin8.

Densitometry analysis of immunoblots was performed using the ImageJ measurement tool. A value of 1 was set for control levels. Background was subtracted from band intensities, and in some cases band intensities were normalized to control bands where indicated.

Zebrafish embryos injections and protein expression analysis

WT TAB-5 zebrafish procedures, care, and husbandry were carried out in compliance with the Guide for Care and Use of Laboratory Animals and approved by the Animal Care and Use Committee of NCI-Frederick (Study Proposal 17-416). RNA and MO injections followed by analysis of 2-day-old ciliated organs were performed as described previously (5). Briefly, full-length human C7orf43 was cloned into pCS2+ vectors, and mRNAs were transcribed using the mMESSAGE mMACHINE kit (Ambion) according to the manufacturer's instructions. Embryos were injected with 250 pg/nl capped mRNAs at the one-cell stage. Knockdowns for *c7orf43* were performed using translation-blocking morpholinos obtained from GENE-TOOLS (Philomath, OR): *C7orf43* MO, 5′-GCGATTCCATC-ATCAACACCATTGA.

For Western blotting, zebrafish embryos lysates were prepared as described previously (5). Briefly, zebrafish embryos were homogenized in lysis buffer (20 mM Tris, pH 8, 137 mM NaCl, 10% glycerol, 1% Triton X-100) enriched with protease inhibitor mixture (Roche Applied Science) and centrifuged for 10 min at 13,000 r.p.m., and supernatants were boiled in sample buffer.

Purification of recombinant proteins and in vitro pulldown assays

Protein expression was induced in BL21 (DE3) *E. coli* cells (Thermo Fisher Scientific) with 200 μM isopropyl 1-thio-β-D-galactopyranoside at 16 °C for 16–20 h. GST and GST-Rabin8 proteins were purified with GSH-agarose beads (Sigma) and further dialyzed with Amicon Ultra-15 centrifugal filter units (Millipore). His-C7orf43 was purified with nickel-nitrilotriacetic acid-agarose beads (Qiagen). *In vitro* pulldown assays were performed by incubating recombinant proteins in low-salt Triton lysis buffer (30 mM Tris-HCl, pH 8.0, 75 mM NaCl, 10% glycerol, 1% Triton X-100 with 5 mM $MgCl_2$) and complete protease inhibitors for 4 h at 4 °C. After three washes with lysis buffer, proteins were eluted with SDS-PAGE sample buffer and analyzed by SDS-PAGE.

Size-exclusion chromatography

Size-exclusion chromatography was performed as described previously (9). Briefly, HEK293 cells were seeded in two 15-cm plates and were grown for 48 h, consolidated into a pellet, and lysed in LAP300 buffer (50 mM HEPES, pH 7.4, 300 mM KCl, 1 mM EGTA, 1 mM $MgCl_2$, 10% glycerol, 0.5 mM DTT, 0.1%

NP-40, protease inhibitors (Roche Applied Science), PhosSTOP (Roche Applied Science). Following sonication and centrifugation, lysates were separated on a Shimadzu liquid chromatography 10ADVP using an Agilent SEC3 300A column. 150-μl fractions were collected and analyzed by Western blotting and subjected to densitometry where indicated.

Statistics

Analyses of statistical data were performed using GraphPad Prism. Data presented are means ± S.E. Two-tailed, unpaired Student's *t* test was applied for comparisons with siControl or as indicated in the figure legends. Significant values shown on graphs are defined as follows: *, $p < 0.05$; **, $p < 0.01$; ***, $p < 0.001$; n.s., not significant.

Author contributions—A. C. performed most experiments with crucial help from C. J. W. (fluorescence imaging); C. I. and J. S. (zebrafish experiments); P. J., M. A. W., and Q. L. (RNAi experiments and immunofluorescence imaging); H. Z. (protein purification; H. Z. and V. W. (immunoprecipitations); M. A. W. and S. S. (HPLC); and S. M. and A. A. P. (secretion assays). H. J. and C. I. discussed the results and commented on the manuscript; C. J. W. and A. C. wrote the paper with suggestions from C. I. and A. A. P. C. J. W. conceived and designed the research.

Acknowledgments—We thank Dr. Thorkel Andressen and Dr. Sudipto Das for assistance with LC-MS analysis and Dr. Dominic Esposito for collection of entry and destination vectors for Gateway Multisite cloning.

References

1. Reiter, J. F., and Leroux, M. R. (2017) Genes and molecular pathways underpinning ciliopathies. *Nat. Rev. Mol. Cell Biol.* **18,** 533–547 CrossRef Medline
2. Waters, A. M., and Beales, P. L. (2011) Ciliopathies: an expanding disease spectrum. *Pediatr. Nephrol.* **26,** 1039–1056 CrossRef Medline
3. Wang, L., and Dynlacht, B. D. (2018) The regulation of cilium assembly and disassembly in development and disease. *Development* **145,** dev151407 CrossRef Medline
4. Sorokin, S. (1962) Centrioles and the formation of rudimentary cilia by fibroblasts and smooth muscle cells. *J. Cell Biol.* **15,** 363–377 CrossRef Medline
5. Lu, Q., Insinna, C., Ott, C., Stauffer, J., Pintado, P. A., Rahajeng, J., Baxa, U., Walia, V., Cuenca, A., Hwang, Y. S., Daar, I. O., Lopes, S., Lippincott-Schwartz, J., Jackson, P. K., Caplan, S., and Westlake, C. J. (2015) Early steps in primary cilium assembly require EHD1/EHD3-dependent ciliary vesicle formation. *Nat. Cell Biol.* **17,** 228–240 CrossRef Medline
6. Insinna, C., Lu, Q., Teixeira, I., Harned, A., Semler, E. M., Stauffer, J., Magidson, V., Tiwari, A., Kenworthy, A. K., Narayan, K., and Westlake, C. J. (2019) Investigation of F-BAR domain PACSIN proteins uncovers membrane tubulation function in cilia assembly and transport. *Nat. Commun.* **10,** 428 CrossRef Medline
7. Knödler, A., Feng, S., Zhang, J., Zhang, X., Das, A., Peränen, J., and Guo, W. (2010) Coordination of Rab8 and Rab11 in primary ciliogenesis. *Proc. Natl. Acad. Sci. U.S.A.* **107,** 6346–6351 CrossRef Medline
8. Sato, T., Iwano, T., Kunii, M., Matsuda, S., Mizuguchi, R., Jung, Y., Hagiwara, H., Yoshihara, Y., Yuzaki, M., Harada, R., and Harada, A. (2014) Rab8a and Rab8b are essential for several apical transport pathways but insufficient for ciliogenesis. *J. Cell Sci.* **127,** 422–431 CrossRef Medline
9. Westlake, C. J., Baye, L. M., Nachury, M. V., Wright, K. J., Ervin, K. E., Phu, L., Chalouni, C., Beck, J. S., Kirkpatrick, D. S., Slusarski, D. C., Sheffield, V. C., Scheller, R. H., and Jackson, P. K. (2011) Primary cilia membrane assembly is initiated by Rab11 and transport protein particle II (TRAPPII) complex-dependent trafficking of Rabin8 to the centrosome. *Proc. Natl. Acad. Sci. U.S.A.* **108,** 2759–2764 CrossRef Medline
10. Xu, S., Liu, Y., Meng, Q., and Wang, B. (2018) Rab34 small GTPase is required for Hedgehog signaling and an early step of ciliary vesicle formation in mouse. *J. Cell Sci.* **131,** jcs213710 CrossRef Medline
11. Nachury, M. V., Loktev, A. V., Zhang, Q., Westlake, C. J., Peränen, J., Merdes, A., Slusarski, D. C., Scheller, R. H., Bazan, J. F., Sheffield, V. C., and Jackson, P. K. (2007) A core complex of BBS proteins cooperates with the GTPase Rab8 to promote ciliary membrane biogenesis. *Cell* **129,** 1201–1213 CrossRef Medline
12. Yoshimura, S., Egerer, J., Fuchs, E., Haas, A. K., and Barr, F. A. (2007) Functional dissection of Rab GTPases involved in primary cilium formation. *J. Cell Biol.* **178,** 363–369 CrossRef Medline
13. Lobo, G. P., Fulmer, D., Guo, L., Zuo, X., Dang, Y., Kim, S. H., Su, Y., George, K., Obert, E., Fogelgren, B., Nihalani, D., Norris, R. A., Rohrer, B., and Lipschutz, J. H. (2017) The exocyst is required for photoreceptor ciliogenesis and retinal development. *J. Biol. Chem.* **292,** 14814–14826 CrossRef Medline
14. Feng, S., Knödler, A., Ren, J., Zhang, J., Zhang, X., Hong, Y., Huang, S., Peränen, J., and Guo, W. (2012) A Rab8 guanine nucleotide exchange factor-effector interaction network regulates primary ciliogenesis. *J. Biol. Chem.* **287,** 15602–15609 CrossRef Medline
15. Chiba, S., Amagai, Y., Homma, Y., Fukuda, M., and Mizuno, K. (2013) NDR2-mediated Rabin8 phosphorylation is crucial for ciliogenesis by switching binding specificity from phosphatidylserine to Sec15. *EMBO J.* **32,** 874–885 CrossRef Medline
16. Bryant, D. M., Datta, A., Rodriguez-Fraticelli, A. E., Peränen, J., Martín-Belmonte, F., and Mostov, K. E. (2010) A molecular network for *de novo* generation of the apical surface and lumen. *Nat. Cell Biol.* **12,** 1035–1045 CrossRef Medline
17. Finetti, F., Patrussi, L., Galgano, D., Cassioli, C., Perinetti, G., Pazour, G. J., and Baldari, C. T. (2015) The small GTPase Rab8 interacts with VAMP-3 to regulate the delivery of recycling T-cell receptors to the immune synapse. *J. Cell Sci.* **128,** 2541–2552 CrossRef Medline
18. Ortiz, D., Medkova, M., Walch-Solimena, C., and Novick, P. (2002) Ypt32 recruits the Sec4p guanine nucleotide exchange factor, Sec2p, to secretory vesicles; evidence for a Rab cascade in yeast. *J. Cell Biol.* **157,** 1005–1015 CrossRef Medline
19. Walia, V., Cuenca, A., Vetter, M., Insinna, C., Perera, S., Lu, Q., Ritt, D. A., Semler, E., Specht, S., Stauffer, J., Morrison, D. K., Lorentzen, E., and Westlake, C. J. (2019) Akt regulates a Rab11-effector switch required for ciliogenesis. *Dev. Cell* **50,** 229–246.e7 CrossRef Medline
20. Schmidt, K. N., Kuhns, S., Neuner, A., Hub, B., Zentgraf, H., and Pereira, G. (2012) Cep164 mediates vesicular docking to the mother centriole during early steps of ciliogenesis. *J. Cell Biol.* **199,** 1083–1101 CrossRef Medline
21. Schou, K. B., Morthorst, S. K., Christensen, S. T., and Pedersen, L. B. (2014) Identification of conserved, centrosome-targeting ASH domains in TRAPPII complex subunits and TRAPPC8. *Cilia* **3,** 6 CrossRef Medline
22. Sacher, M., Shahrzad, N., Kamel, H., and Milev, M. P. (2019) TRAPPopathies: an emerging set of disorders linked to variations in the genes encoding transport protein particle (TRAPP)-associated proteins. *Traffic* **20,** 5–26 CrossRef Medline
23. Waters, A. M., Asfahani, R., Carroll, P., Bicknell, L., Lescai, F., Bright, A., Chanudet, E., Brooks, A., Christou-Savina, S., Osman, G., Walsh, P., Bacchelli, C., Chapgier, A., Vernay, B., Bader, D. M., *et al.* (2015) The kinetochore protein, CENPF, is mutated in human ciliopathy and microcephaly phenotypes. *J. Med. Genet.* **52,** 147–156 CrossRef Medline
24. Patwardhan, D., Mani, S., Passemard, S., Gressens, P., and El Ghouzzi, V. (2018) STIL balancing primary microcephaly and cancer. *Cell Death Dis.* **9,** 65 CrossRef Medline
25. Jayaraman, D., Bae, B. I., and Walsh, C. A. (2018) The Genetics of Primary Microcephaly. *Annu. Rev. Genomics Hum. Genet.* **19,** 177–200 CrossRef Medline
26. Miyamoto, T., Porazinski, S., Wang, H., Borovina, A., Ciruna, B., Shimizu, A., Kajii, T., Kikuchi, A., Furutani-Seiki, M., and Matsuura, S. (2011) Insufficiency of BUBR1, a mitotic spindle checkpoint regulator, causes impaired ciliogenesis in vertebrates. *Hum. Mol. Genet.* **20,** 2058–2070 CrossRef Medline
27. Lipatova, Z., Majumdar, U., and Segev, N. (2016) Trs33-containing TRAPP IV: a novel autophagy-specific Ypt1 GEF. *Genetics* **204,** 1117–1128 CrossRef Medline

28. Lynch-Day, M. A., Bhandari, D., Menon, S., Huang, J., Cai, H., Bartholomew, C. R., Brumell, J. H., Ferro-Novick, S., and Klionsky, D. J. (2010) Trs85 directs a Ypt1 GEF, TRAPPIII, to the phagophore to promote autophagy. *Proc. Natl. Acad. Sci. U.S.A.* **107,** 7811–7816 CrossRef Medline
29. Sacher, M., Barrowman, J., Wang, W., Horecka, J., Zhang, Y., Pypaert, M., and Ferro-Novick, S. (2001) TRAPP I implicated in the specificity of tethering in ER-to-Golgi transport. *Mol. Cell* **7,** 433–442 CrossRef Medline
30. Sacher, M., Jiang, Y., Barrowman, J., Scarpa, A., Burston, J., Zhang, L., Schieltz, D., Yates, J. R., 3rd, Abeliovich, H., and Ferro-Novick, S. (1998) TRAPP, a highly conserved novel complex on the *cis*-Golgi that mediates vesicle docking and fusion. *EMBO J.* **17,** 2494–2503 CrossRef Medline
31. Choi, C., Davey, M., Schluter, C., Pandher, P., Fang, Y., Foster, L. J., and Conibear, E. (2011) Organization and assembly of the TRAPPII complex. *Traffic* **12,** 715–725 CrossRef Medline
32. Bassik, M. C., Kampmann, M., Lebbink, R. J., Wang, S., Hein, M. Y., Poser, I., Weibezahn, J., Horlbeck, M. A., Chen, S., Mann, M., Hyman, A. A., Leproust, E. M., McManus, M. T., and Weissman, J. S. (2013) A systematic mammalian genetic interaction map reveals pathways underlying ricin susceptibility. *Cell* **152,** 909–922 CrossRef Medline
33. Ramírez-Peinado, S., Ignashkova, T. I., van Raam, B. J., Baumann, J., Sennott, E. L., Gendarme, M., Lindemann, R. K., Starnbach, M. N., and Reiling, J. H. (2017) TRAPPC13 modulates autophagy and the response to Golgi stress. *J. Cell Sci.* **130,** 2251–2265 CrossRef Medline
34. Scrivens, P. J., Noueihed, B., Shahrzad, N., Hul, S., Brunet, S., and Sacher, M. (2011) C4orf41 and TTC-15 are mammalian TRAPP components with a role at an early stage in ER-to-Golgi trafficking. *Mol. Biol. Cell* **22,** 2083–2093 CrossRef Medline
35. Wang, W., Sacher, M., and Ferro-Novick, S. (2000) TRAPP stimulates guanine nucleotide exchange on Ypt1p. *J. Cell Biol.* **151,** 289–296 CrossRef Medline
36. Morozova, N., Liang, Y., Tokarev, A. A., Chen, S. H., Cox, R., Andrejic, J., Lipatova, Z., Sciorra, V. A., Emr, S. D., and Segev, N. (2006) TRAPPII subunits are required for the specificity switch of a Ypt-Rab GEF. *Nat. Cell Biol.* **8,** 1263–1269 CrossRef Medline
37. Thomas, L. L., and Fromme, J. C. (2016) GTPase cross talk regulates TRAPPII activation of Rab11 homologues during vesicle biogenesis. *J. Cell Biol.* **215,** 499–513 CrossRef Medline
38. Riedel, F., Galindo, A., Muschalik, N., and Munro, S. (2018) The two TRAPP complexes of metazoans have distinct roles and act on different Rab GTPases. *J. Cell Biol.* **217,** 601–617 CrossRef Medline
39. Yamasaki, A., Menon, S., Yu, S., Barrowman, J., Meerloo, T., Oorschot, V., Klumperman, J., Satoh, A., and Ferro-Novick, S. (2009) mTrs130 is a component of a mammalian TRAPPII complex, a Rab1 GEF that binds to COPI-coated vesicles. *Mol. Biol. Cell* **20,** 4205–4215 CrossRef Medline
40. Wang, N., Lee, I. J., Rask, G., and Wu, J. Q. (2016) Roles of the TRAPP-II complex and the exocyst in membrane deposition during fission yeast cytokinesis. *PLoS Biol.* **14,** e1002437 CrossRef Medline
41. Cai, H., Yu, S., Menon, S., Cai, Y., Lazarova, D., Fu, C., Reinisch, K., Hay, J. C., and Ferro-Novick, S. (2007) TRAPPI tethers COPII vesicles by binding the coat subunit Sec23. *Nature* **445,** 941–944 CrossRef Medline
42. Rossi, G., Kolstad, K., Stone, S., Palluault, F., and Ferro-Novick, S. (1995) BET3 encodes a novel hydrophilic protein that acts in conjunction with yeast SNAREs. *Mol. Biol. Cell* **6,** 1769–1780 CrossRef Medline
43. Molla-Herman, A., Ghossoub, R., Blisnick, T., Meunier, A., Serres, C., Silbermann, F., Emmerson, C., Romeo, K., Bourdoncle, P., Schmitt, A., Saunier, S., Spassky, N., Bastin, P., and Benmerah, A. (2010) The ciliary pocket: an endocytic membrane domain at the base of primary and motile cilia. *J. Cell Sci.* **123,** 1785–1795 CrossRef Medline
44. Malicki, J., Avanesov, A., Li, J., Yuan, S., and Sun, Z. (2011) Analysis of cilia structure and function in zebrafish. *Methods Cell Biol.* **101,** 39–74 CrossRef Medline
45. Wu, C. T., Chen, H. Y., and Tang, T. K. (2018) Myosin-Va is required for preciliary vesicle transportation to the mother centriole during ciliogenesis. *Nat. Cell Biol.* **20,** 175–185 CrossRef Medline
46. Tanos, B. E., Yang, H. J., Soni, R., Wang, W. J., Macaluso, F. P., Asara, J. M., and Tsou, M. F. (2013) Centriole distal appendages promote membrane docking, leading to cilia initiation. *Genes Dev.* **27,** 163–168 CrossRef Medline
47. Yang, T. T., Chong, W. M., Wang, W. J., Mazo, G., Tanos, B., Chen, Z., Tran, T. M. N., Chen, Y. D., Weng, R. R., Huang, C. E., Jane, W. N., Tsou, M. B., and Liao, J. C. (2018) Super-resolution architecture of mammalian centriole distal appendages reveals distinct blade and matrix functional components. *Nat. Commun.* **9,** 2023 CrossRef Medline
48. Liang, Y., Morozova, N., Tokarev, A. A., Mulholland, J. W., Segev, N. (2007) The role of Trs65 in the Ypt:Rab guanine nucleotide exchange factor function of the TRAPP II complex. *Mol. Biol. Cell* **18,** 2533–2541 CrossRef Medline
49. Tokarev, A. A., Taussig, D., Sundaram, G., Lipatova, Z., Liang, Y., Mulholland, J. W., and Segev, N. (2009) TRAPP II complex assembly requires Trs33 or Trs65. *Traffic* **10,** 1831–1844 CrossRef Medline
50. Yip, C. K., Berscheminski, J., and Walz, T. (2010) Molecular architecture of the TRAPPII complex and implications for vesicle tethering. *Nat. Struct. Mol. Biol.* **17,** 1298–1304 CrossRef Medline
51. Cai, H., Zhang, Y., Pypaert, M., Walker, L., and Ferro-Novick, S. (2005) Mutants in trs120 disrupt traffic from the early endosome to the late Golgi. *J. Cell Biol.* **171,** 823–833 CrossRef Medline
52. Yamamoto, K., and Jigami, Y. (2002) Mutation of TRS130, which encodes a component of the TRAPP II complex, activates transcription of OCH1 in *Saccharomyces cerevisiae*. *Curr. Genet.* **42,** 85–93 CrossRef Medline
53. Chen, S., Cai, H., Park, S. K., Menon, S., Jackson, C. L., and Ferro-Novick, S. (2011) Trs65p, a subunit of the Ypt1p GEF TRAPPII, interacts with the Arf1p exchange factor Gea2p to facilitate COPI-mediated vesicle traffic. *Mol. Biol. Cell* **22,** 3634–3644 CrossRef Medline
54. Mojallal, M., Zheng, Y., Hultin, S., Audebert, S., van Harn, T., Johnsson, P., Lenander, C., Fritz, N., Mieth, C., Corcoran, M., Lembo, F., Hallström, M., Hartman, J., Mazure, N. M., Weide, T., *et al.* (2014) AmotL2 disrupts apical-basal cell polarity and promotes tumour invasion. *Nat. Commun.* **5,** 4557 CrossRef Medline
55. Perez, Y., Bar-Yaacov, R., Kadir, R., Wormser, O., Shelef, I., Birk, O. S., Flusser, H., and Birnbaum, R. Y. (2019) Mutations in the microtubule-associated protein MAP11 (C7orf43) cause microcephaly in humans and zebrafish. *Brain* **142,** 574–585 CrossRef Medline
56. Duerinckx, S., Meuwissen, M., Perazzolo, C., Desmyter, L., Pirson, I., and Abramowicz, M. (2018) Phenotypes in siblings with homozygous mutations of TRAPPC9 and/or MCPH1 support a bifunctional model of MCPH1. *Mol. Genet. Genomic Med.* **6,** 660–665 CrossRef Medline
57. Santos-Cortez, R. L. P., Khan, V., Khan, F. S., Mughal, Z. U., Chakchouk, I., Lee, K., Rasheed, M., Hamza, R., Acharya, A., Ullah, E., Saqib, M. A. N., Abbe, I., Ali, G., Hassan, M. J., Khan, S., *et al.* (2018) Novel candidate genes and variants underlying autosomal recessive neurodevelopmental disorders with intellectual disability. *Hum. Genet.* **137,** 735–752 CrossRef Medline
58. Reilly, M. L., Stokman, M. F., Magry, V., Jeanpierre, C., Alves, M., Paydar, M., Hellinga, J., Delous, M., Pouly, D., Failler, M., Martinovic, J., Loeuillet, L., Leroy, B., Tantau, J., Roume, J., *et al.* (2018) Loss of function mutations in KIF14 cause severe microcephaly and kidney development defects in humans and zebrafish. *Hum. Mol. Genet.* **28,** 778–795 CrossRef Medline
59. Daly, O. M., Gaboriau, D., Karakaya, K., King, S., Dantas, T. J., Lalor, P., Dockery, P., Krämer, A., and Morrison, C. G. (2016) CEP164-null cells generated by genome editing show a ciliation defect with intact DNA repair capacity. *J. Cell Sci.* **129,** 1769–1774 CrossRef Medline
60. Li, C., Luo, X., Zhao, S., Siu, G. K., Liang, Y., Chan, H. C., Satoh, A., and Yu, S. S. (2017) COPI-TRAPPII activates Rab18 and regulates its lipid droplet association. *EMBO J.* **36,** 441–457 CrossRef Medline
61. Torres, J. Z., Miller, J. J., and Jackson, P. K. (2009) High-throughput generation of tagged stable cell lines for proteomic analysis. *Proteomics* **9,** 2888–2891 CrossRef Medline
62. Westlake, C. J., Junutula, J. R., Simon, G. C., Pilli, M., Prekeris, R., Scheller, R. H., Jackson, P. K., and Eldridge, A. G. (2007) Identification of Rab11 as a small GTPase binding protein for the Evi5 oncogene. *Proc. Natl. Acad. Sci. U.S.A.* **104,** 1236–1241 CrossRef Medline
63. Das, S., Bosley, A. D., Ye, X., Chan, K. C., Chu, I., Green, J. E., Issaq, H. J., Veenstra, T. D., and Andresson, T. (2010) Comparison of strong cation exchange and SDS-PAGE fractionation for analysis of multiprotein complexes. *J. Proteome Res.* **9,** 6696–6704 CrossRef Medline